

2 - p(mix)

UNIVERSITY OF SOUTHERN CALIFORNIA  
2025 ZONAL AVENUE  
LOS ANGELES, CALIFORNIA 90033

DEPARTMENT OF  
CONTRACTS AND GRANTS  
(MEDICAL CAMPUS OFFICE)

TELEPHONE (213) 225-1511  
EXTENSION 432 OR 433

January 16, 1973

IN REPLY REFER TO: 063013-MC/1449

National Aeronautics Space Administration  
Contracts Office  
Code DHC-2  
Washington, D.C. 20546

ATTENTION: J. B. Phillips, Jr.  
Contracts Officer

SUBJECT: Final Report

REFERENCE: Contract No. NSR 05-018-087 - J. P. Meehan/J. P. Henry -  
Principal Investigator

"Observation of Arterial Blood Pressure of the Primate"

Gentlemen:

The University of Southern California, on behalf of Dr. J. P. Meehan, is pleased to forward the enclosed Final Report on the above referenced contract.

Additional copies distribution in accordance with the attached list.'

If you should have any further questions, please feel free to contact me at the above address.

Very truly yours,

Sam Cecil, Assistant Director  
Department of Contracts and Grants  
Medical Campus  
University of Southern California

SC:ar  
cc: Dr. Meehan

UNIVERSITY AFFAIRS

Reproduced by  
NATIONAL TECHNICAL  
INFORMATION SERVICE  
US Department of Commerce  
Springfield, VA. 22151

UN 07 5 87 MHC

(NASA-CR-131890)	OBSERVATION OF ARTERIAL	N73-21980
BLOOD PRESSURE OF THE PRIMATE	Final	
Report (University of Southern Calif.)		
77 p	CSCL 06C	Unclas
		G3/04 17153

N O T I C E

THIS DOCUMENT HAS BEEN REPRODUCED FROM THE BEST COPY FURNISHED US BY THE SPONSORING AGENCY. ALTHOUGH IT IS RECOGNIZED THAT CERTAIN PORTIONS ARE ILLEGIBLE, IT IS BEING RE-LEASED IN THE INTEREST OF MAKING AVAILABLE AS MUCH INFORMATION AS POSSIBLE.

National Aeronautics Space Administration  
Contracting Office  
Code DHC-2  
Washington, D. C. 20546  
1 Copy

National Aeronautics Space Administration  
Technical Reports Office  
Office of University Affairs  
Code 1  
Washington, D.C. 20546  
1 Repo. and 10 Copies

National Aeronautics Space Administration  
Manager Advanced Projects & Technology  
Code SB  
Washington, D.C. 20546  
2 Copies

G. Max Irving, Administrative Contracting Officer  
Department of the Navy  
Office of Naval Research  
1030 East Green Street  
Pasadena, California 91101  
1 Copy

Details of illustrations in  
this document may be better  
studied on microfiche

FINAL REPORT

January 9, 1973

NASA Contract Number NSR 05-018-087

(U.S.C. Number 53-5137-1449)

usc-


Title: Observation of Arterial Blood Pressure of the Primate

Principal Investigators: J. P. Meehan, M.D.  
J. P. Henry, M.D.

Project Director: R. D. Rader

UNIVERSITY OF SOUTHERN CALIFORNIA  
School of Medicine  
Department of Physiology  
Environmental Physiology Laboratories  
Los Angeles, California 90007

  
J. P. Meehan, M.D.

  
J. P. Henry, M.D.

## P r e f a c e

This report is sectioned into a summary, a description of the hardware developed, a description of research applications in renal hemodynamics and the conclusions.

The sections on the development and application are drawn from the texts of two papers prepared in this laboratory. Section II is essentially the text from R. D. Rader's "Telemetry Implants" for the book, Clinical Telemetry, edited by Cesar A. Caceres for Academic Press publication in 1973. Section III is principally comprised of material from the paper "Renal Parameter Estimates in Unrestrained Dogs," by R. D. Rader and C. M. Stevens. The latter paper will be submitted for publication to an appropriate journal.

# C o n t e n t s

- I. Summary
- II. Development of an Implantable Telemetric Data Acquisition System
  - A. Introduction
  - B. Design Problems and Goals
  - C. Instrumentation Design
    - 1. Carrier and Subcarrier Oscillator
    - 2. Power Controller and Voltage Regulator
    - 3. Blood Pressure Signal Conditioner
    - 4. Flow Concept
    - 5. Flow Circuit
  - D. Stability Consideration
  - E. Packaging Technique
  - F. Evaluation
  - G. Circuit Values
  - H. References
- III. Cardiovascular Research Applications
  - A. Introduction
  - B. Renal Hemodynamic Model
  - C. Experimental Application in Renal Functions
  - D. Pitfalls and Problems
  - E. Discussion
  - F. References
- IV. Conclusions

## I. Summary

The work statement for NASA Contract No. NSR 05-018-087 committed the University of Southern California Department of Physiology to a continuing program of research directed toward the development of physiological instrumentation, surgical procedures, measurement and data analysis techniques, and a definition of flight experiments to determine the effects of prolonged weightlessness on the cardiovascular system of subhuman primates. The Work Statement, submitted in the original proposal and accepted as a part of the contract performance, divided the research into experiments with both free and with partially restrained animals.

### A. Contract Requirements

Specific contractual tasks were:

Task Number One. To continue development and testing of implantable sensors and telemetry systems to detect blood pressure, blood flow, vascular dimensions, and biopotential.

Task Number Two. To continue experimental evaluation of sensor and telemetry systems and to identify acceptable implant sites by a program of experiments on animals which are affixed with implantable instrumentation systems.

Task Number Three. To acquire baseline data on possible flight species by a program of experiments designed to acquire cardiovascular data in relation to the subject's total environment.

Task Number Four. To investigate hemodynamics, both systemic and renal, to the adjustments seen in man and to formulate a series of vascular measurements that would provide the best dynamic record of blood volume shifts and hemodynamic responses to weightlessness and simulated weightlessness.

Task Number Five. To compare cardiovascular data obtained during the experiments with central nervous system (CNS) data so that possible meaningful relationships between CNS and autonomic nervous system function as revealed by the proposed cardiovascular measures could be recognized and evaluated.

The investigation employing restrained and unrestrained subjects had a common goal consisting of the development and application of sensors which would reliably and accurately

detect parameters, such as blood pressure, blood flow, and vascular dimensions. Stable, reliable sensors clearly bear a very direct relationship to the outcome of any measurement and therefore considerable work in developing the sensors was done. The commitment to develop instruments to monitor unrestrained subjects resulted in the development of a totally implantable telemetry system that will operate for a duration in excess of one year.

#### B. Contract Performance

Performance summaries for each respective task are listed below:

Task Number One Performance--Development. The main development efforts were directed toward improving the sensors and electronics necessary to obtain measurements of blood flow, blood pressure, and vascular dimensions. Emphasis was placed on developing and testing blood flow probes and on further reduction in power consumption and size of implanted telemetry systems. Development of techniques to obtain cardiovascular dimensions was completed through a breadboard stage. Blood pressure, blood flow, biopotential, and power control electronics assemblies were designed and tested and have been evaluated by their use in chronic telemetry experiments. Ground station electronics necessary for conditioning, analyzing, and recording information were also developed and used.

Task Number Two Performance--Evaluation. In conducting the evaluation of the sensors and electronics assemblies extensive experience was gained in applying the sensors and in obtaining data from partially restrained subjects where sensor leads communicate through the skin. Blood pressure sensors of the available commercial variety have undergone considerable testing and were found to lack long term stability. Immediate success in the area of blood flow measurements was delayed because of structural failure of the commercially available ultrasonic flow probes. To solve this problem we undertook the development and fabrication of our own probes; these probes have now undergone long term testing in telemetry implants. As yet there remains an inability to precisely calibrate flow for in vivo application. The results of our efforts in developing packaging and sealing techniques for implanted devices have been good. One telemetry system survived a total implant of four months and was removed only because of the failure of blood flow measurements. A second



implant transmitted data for a period of 4.5 months. Failure appeared to be a combination of lead breakage in the flow probe and a dead battery. Typical failure is due to lead breakage.

Task Number Three Performance--Data Acquisition. Since national policies reduced the priority of orbital animal experiments, dogs were used during the entire development and applications as other suitable subjects were unavailable. Experimental efforts with dogs have included measurements of arterial pressure, blood flow at various sites, and vascular dimensions. Several dogs have been instrumented with totally implanted pressure and flow telemetry systems. Excellent results in the area of pressure and flow measurements have been obtained.

Task Number Four Performance--Cardiovascular Hemodynamics. Experimental application dealt mainly with systemic and renal cardiovascular studies. A means of measuring renal hemodynamics by the use of blood flow and pressure dynamics was conceptualized and evaluated. Because of the major role the renal system plays in regulating body fluids and vascular pressures, several studies were conducted on renal hemodynamics. Application of this technique may permit an assessment of renal function in weightlessness which has considerable advantage relating to size, power, and weight.

Task Number Five Performance--Cardiovascular and CNS Data. The intent was to associate with the UCLA Brain Research Institute in performing this portion of the contractual efforts. The degree to which this Task Number Five was accomplished was limited by the national policy curtailing animal research in space. To a lesser degree this effort was accomplished in our own laboratories in the work done on renal hemodynamics. In this task subjective measurements of neuro-activity was correlated with renal hemodynamic responses.

NASA Contract Number

NSR 05-018-087

## II. Development of an Implantable Telemetric Data Acquisition System

### A. Introduction

### B. Design Problems and Goals

### C. Instrumentation Design

#### 1. Carrier and Subcarrier Oscillator

#### 2. Power Controller and Voltage Regulator

#### 3. Blood Pressure Signal Conditioner

#### 4. Flow Concept

#### 5. Flow Circuit

### D. Stability Consideration

### E. Packaging Technique

### F. Evaluation

### G. Circuit Values

### H. References

## II. Development of an Implantable Telemetric Data Acquisition System

### A. Introduction

Care must be exercised in conducting any measurement in order to insure that the inclusion of the sensing device within the media does not excessively disturb the quantities being measured. An additional problem arises in conducting measurements on animals, as both the act of introducing the animal into an experimental situation and the often traumatic application of the sensing and measuring device to the subject can produce an emotional reaction which influences the value of the parameters being investigated. To minimize this emotional reaction, drugs are often administered with the result that the parameter under investigation may be significantly altered. In many cases neither option, the application of the measuring device without the benefit of drugs, nor the administration of drugs to control the subject's reaction to the application of the device yields a valid experimental situation. An escape from this experimental dilemma is available in the use of biotelemetry. The subject can then be instrumented under anesthesia and after sufficient time for recovery can be monitored under more natural conditions. The application of telemetry as a tool for improving measurement techniques is expanding and is currently credited as a major means of acquiring data from near-normal, unrestrained, unanesthetized animals subjects (Rader et al., 1968).

Experimental techniques in unrestrained ambulatory animals are further improved by the use of totally implanted telemetry devices. It is the problem of the designer to achieve a telemetry device meeting conditions relating to size, operating life, accuracy, and reliability which satisfies the experimental requirements. The necessity for implant often imposes stringent design conditions. An equipment package size compatible with subject size is a major controlling factor. With a fixed package size, operating life can only be increased by limiting power consumption; thus the use of low power electronics is necessary and some form of transmitter control is indicated. Reliable maintenance-free operation is also very important; as once the unit is implanted, repair can generally be conducted only by entirely removing the implanted electronics package. Measurement stability is also of major importance as frequent calibration cannot be readily performed once the implant has been achieved.

In an efficient measuring system, parameter selection is often made on the basis of maximum information yield relative to constraints such as minimum power expenditure, acceptable accuracy, and minimization of size. In cardiovascular research parameter selection is biased by the fact that knowledge of blood pressure and blood flow is required for appreciating the hemodynamics of the entire circulation or of any particular segment. Measurement of these two parameters yields considerable direct information and other parameters can be calculated. In addition to heart rate, dynamic pressure measurements yield information about the heart contractility and the elasticity of the vessels. Dynamic blood flow measurements conducted on the ascending aorta yield cardiac output in liters per minute. From the ratio of mean pressure to mean flow an estimate of mean flow resistance can be obtained; and since this resistance is modulated in part by nervous system inputs, a feeling for the involvement of the central nervous system in cardiovascular regulation can be developed. Data analysis is further improved by electronic means of achieving division, integration, and differentiation.

Totally implantable pressure-sensing techniques have been quite well developed in the last decade and currently enjoy modest application in biological research. On the other hand, totally implantable techniques for measuring blood flow have not been equally well developed. The currently popular electromagnetic techniques require considerable power and extensive circuitry and yield a very low-level voltage analog of flow. Long term stability is inadequate to allow definite placement of zero flow without occlusion. The sensitivity also varies with vessel wall thickness and hematocrit value. On the other hand, ultrasonic techniques are comparatively new to the field of blood flow measurement and do not enjoy the confidence extended to electromagnetic means. A major criticism leveled at all existing ultrasonic measuring techniques relates to the inability to quantify the results.

Less basic problems but nevertheless critical ones also exist (Rushmer, 1966). For example, in acute application the ultrasonic probes often lose contact with the vessel wall and produce erratic readings. Acute use of the probes is possible by careful application of gels or foams which insure good contact of the crystals with the vessel wall. On the positive side, the probes are lighter, conditioning circuitry is often not extensive, power requirements are low, and the unamplified signal level is for some versions two orders of magnitude above that produced by electromagnetic techniques. Zero

stability, though not optimum, is acceptable. For chronic application problems associated with poor vessel wall contact are obviated by the tissue growth in and around the probe. Calibration for either the electromagnetic or ultrasonic technique is tedious, difficult, and generally inaccurate, and therefore it is not the deciding factor in selecting the optimum sensing device.

The ultrasonic technique was preferred in our laboratories for extensive implant application principally because of the low power requirements, lighter probe, and less extensive circuitry requirements. The specific ultrasonic technique used in this development was selected over others because of its inherent simplicity and its comparatively greater basic analog signal level.

#### B. Design Problems and Goals

The effectiveness of the analysis of the cardiovascular system is greatly enhanced by making simultaneous measures of flow and pressure, for when they are taken together they yield impedance, a third important variable. Specifically flow is equal to pressure divided by impedance; thus if pressure and flow are measured, the impedance can be calculated. The use of implanted sensors to detect flow and pressure and the use of external electronics to transmit this data to remote recording sites is quite common (Franklin et al., 1971; Rader et al., 1967). However the technique has several problems associated with it. The possibility of infection where leads emerge through the skin is high. A degree of control is possible by the use of antibiotics and by aseptic techniques. Protection of the sensor leads and attached equipment is very difficult. A solution to these troublesome problems is not an absolute requirement as extreme care will allow useful data to be obtained over a considerable duration. However the application of an implantable telemetry device that eliminates these problems without creating added problems has a clear experimental advantage. Fortunately in practice few new problems are created by total implants. A potential hazard is tissue reaction to the implant; however, in actual practice it has not been a problem. Many materials acceptable for implant have been identified and the equipment size can be reduced to acceptable limits (Brown et al., 1971; Rader, 1971). At the crux of the matter are the problems of obtaining seals at connectors and sensors and achieving acceptable stability with low power expenditure. The matter of sealing can be solved by good practices. The remaining

problems are related to achieving sufficient operating life with the limited energy available to qualify the system for a long term implant and to realizing sufficient stability to make the device useful. It is to this last problem that the designer must address himself.

The current state of energy sources limits the total operating life to a rather short period if continuous operation is attempted. Fortunately the nature of many experiments does not require continuous data. Sufficient clarity can often be obtained by sampling; thus one minute of data each hour might be adequate. Not only does this prolong the useful lifetime of the device, but it trims the data to a manageable quantity. With the expedient of controllable or at least programmed transmission a package size acceptable for implant and operational for several years can be achieved. Representative techniques for implantable systems are presented by Rader (1971) and Fryer (1970).

The design problems are not simple and as in most situations compromises are necessary. To extend the operating life micropower circuitry must be employed. In addition to limiting transmission time, other current-saving techniques such as duty cycling of amplifiers and oscillators must also be incorporated. For many cardiovascular measurements integrated circuits of sufficiently low power consumption are not available, and one must resort to a discrete component approach or become involved in a hybrid development which often produces only a small decrease in volume and power consumption at considerable economic cost. The discrete component approach is necessary for many developments.

There is an abundance of telemetry techniques many of which have a particular advantage for certain applications. An FM/FM mode was employed in the past and developed under government contracts with the requirement that the standard IRIG systems be used. The directive was sound as standard receiving and demodulating equipment exists and the number of channels required for effective animal experiments does not exceed that available. The trend was thus established and no compelling reason has existed to force a change. A typical data channel consists of a sensor, a signal conditioner, and a sub-carrier oscillator. Common to all channels is a carrier oscillator, a power supply, a regulator, and a power controller. The stability of all modules in the package influences either the measurement accuracy or the reliability.

Stability, though often incompatible with low current operation, is of critical importance as calibration cannot readily be performed once implant has been achieved. Thus the stability of the slope (sensitivity) and the intercept (baseline) must be held to acceptable limits for months. Sensor aging, component aging, and supply voltage variations contribute to instability. Negative feedback can be employed to control component aging and voltage regulation can be used to reduce the sensitivity to supply voltage variation. Realization of sensor stability is definitely the most difficult problem and can be dealt with effectively only by sound sensor design and application. This problem is further complicated by the requirement for small size sensors and their use in a chemically hostile environment. Thermal effects can often be eliminated by specific compensation of the combined sensor and circuitry but there is no easy solution to the long term drift problem.

### C. Instrumentation Design

In this development one of the more important factors has been the realization of low current operation in conjunction with small size and good thermal and time stability. The end product of the electronic development has been a frequency modulated subcarrier oscillator proportional to either pressure, flow, or biopotential signals.

The cardiovascular implant system utilizes one 9.8-volt, 160 milliamperes-hour mercury cell battery with a voltage regulator. Transmission is initiated by an RF signal and terminates automatically after a preset interval. A potential of 800, 8-minute transmission episodes is available. By this expedient in concert with the use of low power electronics an experiment with a potential duration in excess of a year can be conducted.

1. Carrier and Subcarrier Oscillator. The carrier oscillator is a single stage LC oscillator displacing approximately 0.15 cubic inches (Fig. 1). It requires less than 1 milliamperes at 6 volts to deliver sufficient power for a substantial transmission distance. A combination shield and antenna developed for the oscillator makes it relatively immune to frequency changes caused by proximity to objects. Average handling produces frequency changes in the order of 40 kilohertz at center frequencies between 215 and 260 megahertz. A temperature change from 50 to 120 degrees Fahrenheit causes a frequency shift of approximately 150 kilohertz.

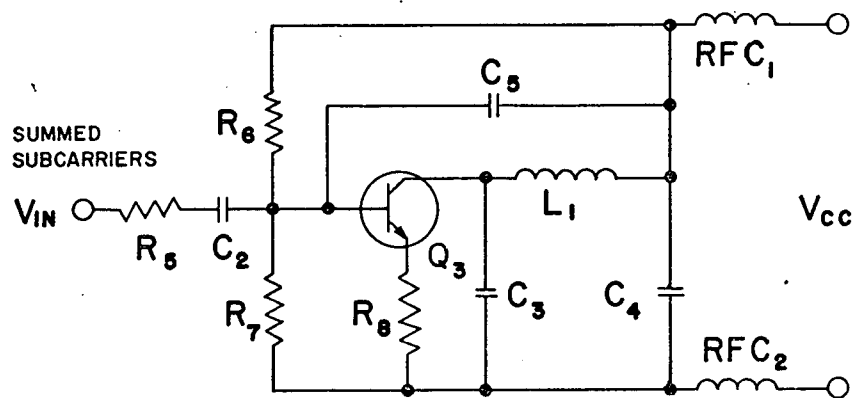


Figure 1. Circuit Schematic for Radio Frequency Oscillator.



Complete immersion in water shifts the frequency by 40 kilohertz. In most cases the shift is well within the automatic frequency control of the receiver used. The oscillator will operate with all standard IRIG subcarrier frequencies. The immunity of the oscillator to proximity effects allows the transmitter to be placed directly on or within the subjects.

Special IRIG frequency subcarrier oscillators were employed which were independent of temperature, supply voltage, and load changes and have inherent frequency modulation limits for prevention of overmodulation into adjacent channels (Rader and Griswold, 1965). The oscillator is functionally illustrated in Fig. 2 (top). The characteristic equation for the oscillator can be found by considering each loop separately and adding the results. The loop equations in terms of transfer functions and gain factors are:

$$\begin{aligned} A &= (A + B) G_1 K_1 \\ B &= (A + B) G_2 K_2 \end{aligned} \tag{1}$$

Addition of these equations results in

$$K_1 G_1 + K_2 G_2 = 1 \tag{1a}$$

Oscillation is possible when Eq. 1a is true. Gain factors  $K_1$  and  $K_2$  can be controlled and  $G_1$  and  $G_2$  are frequency-dependent transfer functions. The frequency at which Eq. 1a is zero is influenced by both the gain factors and the property of the transfer functions. With fixed transfer functions single-ended modulation is possible by control of either  $K_1$  or  $K_2$  and double-ended modulation possible by control of both  $K_1$  and  $K_2$ . In the circuit (Fig. 2, center) the gain is controlled by the bias on transistors  $Q_1$  and  $Q_2$ . Equation 1a also reveals limit frequencies beyond which the oscillator cannot be modulated regardless of the variation of  $K_1$  or  $K_2$ . These limit frequencies are defined by transfer functions  $G_1$  and  $G_2$ . Proper selection of  $G_1$  and  $G_2$  prevents overmodulation into adjacent channels and subsequent loss of information. A brief analysis of an ideal circuit similar to the one shown in Fig. 2 is undertaken below. The transfer function for the parallel T networks (Landee et al., 1957) can be written as

Figure 2. Subcarrier Oscillator.

(Top) Functional Diagram

(Center) Circuit Diagram

(Bottom) Performance Curve

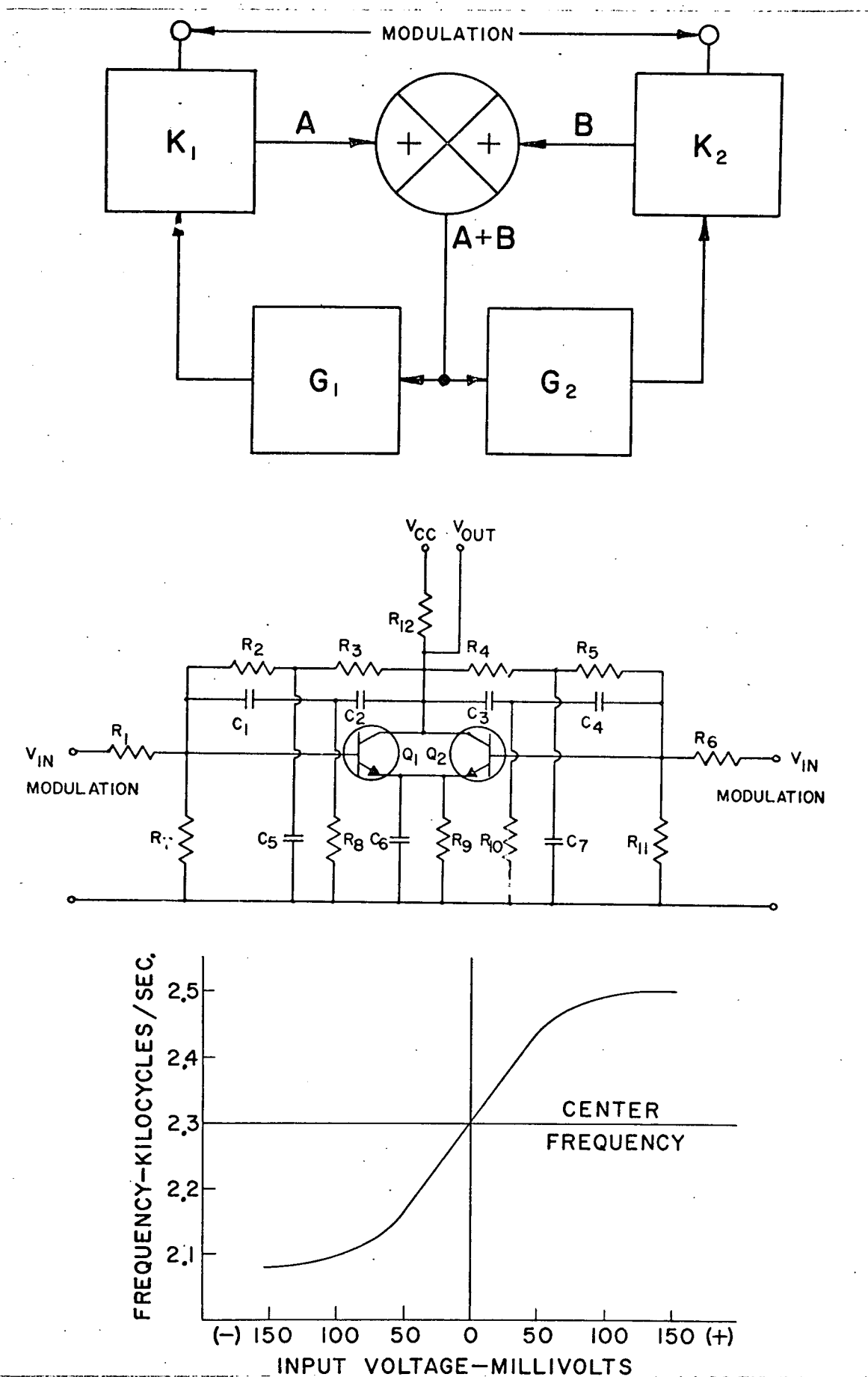


Figure 2

$$\begin{aligned}
 G_1 &= \frac{E_0}{E_1} = \frac{X(\omega) + jB}{X(\omega) + jC} \\
 G_2 &= \frac{E_0}{E_2} = \frac{Y(\omega) + jB}{Y(\omega) + jC}
 \end{aligned}
 \tag{2}$$

where B and C are constants.

The definitions of X and Y are

$$\begin{aligned}
 X &= \frac{\omega_1}{\omega} - \frac{\omega}{\omega_1} ; \quad \omega_1 = 1/R_1 C_1 \\
 Y &= \frac{\omega_2}{\omega} - \frac{\omega}{\omega_2} ; \quad \omega_2 = 1/R_2 C_2
 \end{aligned}
 \tag{3}$$

Substitution of these parameters into Eq. 1a gives:

$$K_1 \frac{X + jB}{X + jC} + K_2 \frac{Y + jB}{Y + jC} = 1
 \tag{4}$$

For this equation to be true, the left side must have no imaginary term. Equating the imaginary part of Eq. 4 to zero gives

$$K_1 X (B - C) (Y^2 + C^2) + K_2 Y (B - C) (X^2 + C^2) = 0
 \tag{5}$$

A general solution to Eq. 5 is difficult; therefore three special cases will be considered.

$$\text{Case 1} \quad K_2 = 0 \quad K_1 \neq 0$$

Setting  $K_2$  to zero in Eq. 4 and equating the imaginary part of the left side to zero gives

$$X (B - C) = 0
 \tag{6}$$

If  $(B - C)$  is not zero, then X must be zero. Therefore,

$$\frac{\omega_1}{\omega} - \frac{\omega}{\omega_1} = 0
 \tag{7}$$

Solution of Eq. 7 gives

$$\omega = \omega_1$$

Case 2       $K_1 = 0 \quad K_2 \neq 0$

By the same approach it can be shown that  $\omega = \omega_2$  when  $K_1 = 0$ .

Case 3       $K_1 = K_2 = K$

When  $K_1 = K_2 = K$ , Eq. 5 simplifies to

$$K (B - C) (X + Y) (X Y + C^2) = 0 \quad (8)$$

One solution is found by allowing  $X + Y$  to equal zero.

This condition results in

$$\frac{\omega_1}{\omega} - \frac{\omega}{\omega_1} + \frac{\omega_2}{\omega} - \frac{\omega}{\omega_2} = 0 \quad (9)$$

Solution of Eq. 9 gives

$$\omega = \sqrt{\omega_1 \omega_2} \quad (10)$$

The curve in Fig. 2 (bottom) illustrates the modulation sensitivity and limit frequencies. To provide good linearity the limit frequencies are generally set at about the  $\pm 10\%$  point on the standard IRIG channels. Frequency variation due to temperature variation is small due to the use of temperature insensitivity components. The oscillator requires 100 microamperes at 6 volts. The unloaded output is a 3-volt sinusoidal signal and requires little filtering for elimination of higher harmonics. The transfer functions can easily be designed to produce oscillation at center frequencies from 400 Hz to 22 KHz with limit frequencies at  $\pm 10\%$  of center frequency. Frequency-to-voltage conversion has been achieved by use of the standard commercial discriminators or by the use of phase-lock loop systems built around available integrated phase-lock loop circuits.

2. Power Controller and Voltage Regulator. In order to realize reliable implantable devices that will operate for several months it is necessary to limit transmission time to a small percentage of the intended implant life. One solution is to employ a radio frequency actuated switch that enables transmission time to be controlled by the investigator. Transmitted energy is received and detected by an inductance capacitance tuned circuit in the base circuit of a high gain amplifier. The amplifier turns on a silicone control switch which remains on for a predetermined interval. This mode of operation allows command of transmission and insures against rapid battery decay due to accidental turn on by extraneous sources.

Figure 3 (top) illustrates the circuit developed for the control function. Transistors  $Q_1$  and  $Q_2$  comprise a high gain amplifier which amplifies the signal induced across the tank circuit. This signal is rectified and employed to turn on  $SCS_1$  to initiate transmission. Capacitor  $C_4$  then charges, and through  $Q_3$ , this charge turns on  $SCS_2$ , which through its influence on  $Q_4$  turns the entire system off and terminates transmission. The function of  $D_4$  is to remove the remaining charge on  $C_4$  after transmission is terminated. This allows a near-normal transmission time if the system is immediately reactivated. The duration of transmission is controlled by  $R_9$  and can be set conveniently anywhere between a few seconds and 20 minutes.

The regulator in the circuit is shown in detail at the bottom in Fig. 3. Basically the regulator consists of a high-gain, low power amplifier referenced to a constant voltage source. Transistor  $Q_1$  is employed as a series regulator which in turn is controlled by  $Q_2$  and  $Q_3$ .  $Q_2$  senses any voltage change across the load and through its influence on  $Q_3$  and  $Q_1$  corrects for this change. The majority of the current used by the regulating amplifier is directed through the voltage reference, eliminating a separate current path for this function.  $Q_4$  compensates for a 50 through 120 degree Fahrenheit environmental temperature change. The regulator consumes approximately 1.5 milliwatts of power.

3. Blood Pressure Signal Conditioner. Blood pressure is detected by the use of chronically implanted miniature pressure sensors (Konigsberg, 1966). The sensor body is unalloyed titanium 6.5 millimeters in diameter and 1 millimeter thick. This material is highly corrosion-resistant, allowing long term direct contact with body fluids. Four

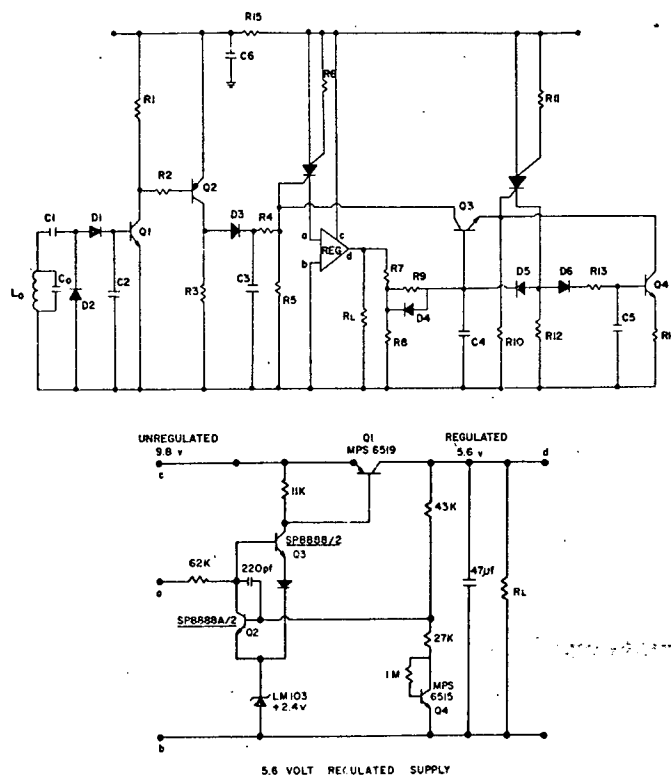


Figure 3. (Top) Circuit Schematic of Radio Controlled Switch.  
(Bottom) Circuit Schematic of Voltage Regulator.

semiconductor strain gauges connected in a conventional four-arm bridge are bonded to the inner surface of the small pressure-sensing diaphragm. Positive pressure on the face of the transducer causes resistance changes that are transformed to a voltage change. The sensor is quite sensitive producing approximately 30 mv/300 mm Hg, when used as suggested by the manufacturer. Its frequency response is well in excess of that required to obtain dynamic blood pressure measurements and its temperature characteristics can be determined and properly handled.

Figure 4 illustrates a circuit schematic that transforms blood pressure variations to voltage variations and sequentially produces frequency modulation of a subcarrier oscillator proportional to pressure. Conditions dictating the circuit design relate mainly to power consumption and reliability. Modest power consumption in concert with high sensitivity was achieved by pulsed operation of the resistance transducer and by utilization of low power auxiliary circuitry.

The circuit consists of a differential input voltage-controlled oscillator with active elements  $Q_5$  and  $Q_6$ ; a pulse generator consisting of active components  $Q_1$ ,  $SCS_1$ , and  $Q_4$ ; and a pulse-amplifying circuit consisting of  $Q_2$  and  $Q_3$ . The output of the voltage-controlled oscillator turns  $SCS_1$  on, which turns  $Q_4$  on, placing the supply voltage across the pressure sensor. Transistor  $Q_1$  turns on after a delay established by the RC time constant and turns  $SCS_1$  off. The effect is then an application of a narrow voltage pulse to the pressure sensor on each positive excursion of the voltage-controlled oscillator output. The difference between the pulse levels at the output of the pressure sensor is amplified by  $Q_2$  and  $Q_3$  and filtered by the RC networks connected to the collectors. The resultant DC voltage which is proportional to pressure applied to the transducer is employed to modulate the voltage-controlled oscillator. The major advantages of this mode of operation are high sensitivity, low current operation, and the realization of overmodulation protection by the use of a subcarrier with frequency limits.

4. Flow Concept. The block diagram at the top in Fig. 5 illustrates a prototype system which is considered first to aid in understanding the concept (Rader, 1971; Plass, 1964). Piezoelectric crystals resonant at 5 MHz are positioned diagonally across a flow section. The crystals are excited in phase opposition by a continuous 5 MHz signal. The ultrasonic energy generated by crystal  $X_1$  and transmitted



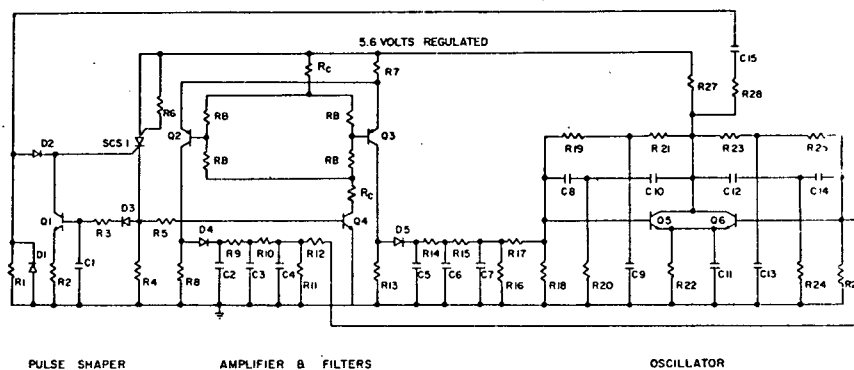


Figure 4. Blood Pressure Signal Conditioner Schematic. Resistances RB are the four elements of the pressure sensor.

downstream causes a mechanically-induced voltage to sum with the electrical excitation voltage on crystal  $X_2$ . The same is true for the energy generated by  $X_2$  and received by  $X_1$ . These cross-coupled signals are either delayed or advanced in time and are therefore modulated in phase relative to the excitation voltage in proportion to flow velocity. Specifically in an ideal case where exact balance exists and only the excitation voltage and the first incident term are considered voltages  $e_1$  and  $e_2$  are:

$$\begin{aligned} e_1 &= V K_e \cos \omega t - K_e K_s V \cos (\omega t + \gamma + \theta) \\ e_2 &= V K_e \cos \omega t + K_e K_s V \cos (\omega t + \gamma - \theta) \end{aligned} \quad (11)$$

where the cross-coupled mechanically-induced components are:

$$\begin{aligned} &- K_e K_s V \cos (\omega t + \gamma + \theta) \quad (\text{energy from } X_2 \text{ impinging on } X_1) \\ &+ K_e K_s V \cos (\omega t + \gamma - \theta) \quad (\text{energy from } X_1 \text{ impinging on } X_2) \end{aligned} \quad (12)$$

Where the parameter  $K_e$  is an attenuation factor related to the impedances of the source and the crystals, and the constant  $K_s$  is an attenuation factor related to distance and to the material between crystals and to the  $Q$  of the crystals,  $\theta$  is the phase shift caused by the flow; and  $\gamma$  is the phase shift related to the probe geometry. The idealized output voltage is then

$$e_s = e_1 + e_2 = 2 K_s K_e V \sin \theta \sin (\omega t + \gamma) \quad (13)$$

The magnitude of the signal voltage is thus a function of  $\sin \theta$ , the coupling coefficient  $K_s$ , and the effective crystal drive voltage  $K_e V$ . The value of  $\theta$  and  $\gamma$  can be derived by consideration of the geometry and the flow velocity. In particular, as derived from Fig. 5, the time required for energy to propagate from crystal  $X_1$  to  $X_2$  is:

$$T_{1-2} = \int_0^{\ell} \frac{dx}{C} + \int_{\ell}^{d-\ell} \frac{dx}{C + v \cos} + \int_{d-\ell}^d \frac{dx}{C} \quad (14)$$

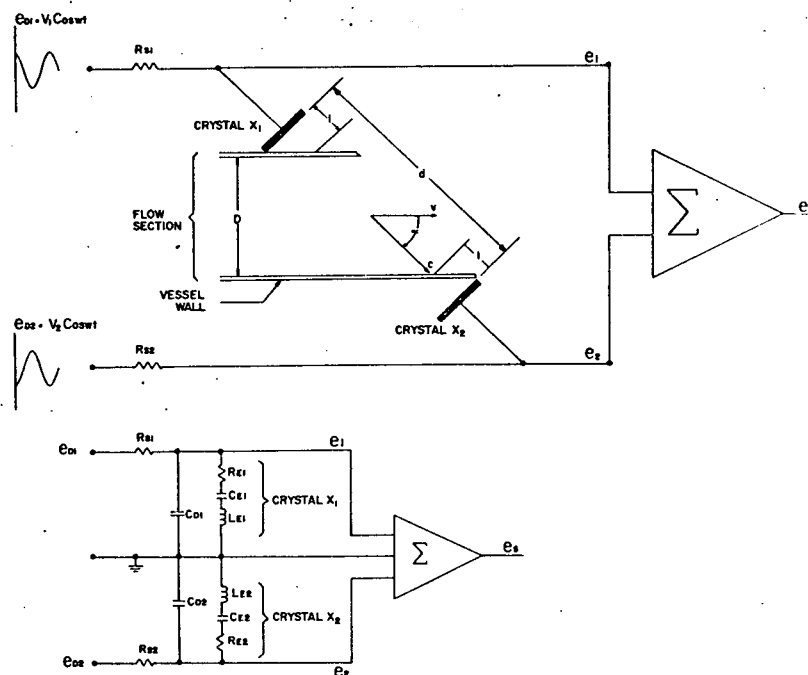


Figure 5. Blood Flow Measuring Concept and Approximate Crystal Equivalent Circuit.

Where  $C$  is the velocity of the acoustical energy in the medium,  $\alpha$  is the angle between the flow velocity and the ultrasonic energy propagation direction,  $v$  is the velocity of blood flow which for purposes of analysis is assumed to be blunt, and  $d$  the distance between crystal faces, and  $\ell$  the distance from inside of the vessel to each crystal face. Division of

$$\frac{1}{C + v \cos \alpha} \quad (15)$$

results in

$$\frac{1}{C} \left[ 1 - \frac{v \cos \alpha}{C} + \left( \frac{v \cos \alpha}{C} \right)^2 - \left( \frac{v \cos \alpha}{C} \right)^3 \dots \right] \quad (16)$$

By valid assumption that

$$\frac{v \cos \alpha}{C} \ll 1 \quad (17)$$

the squared and higher power terms of the series can be neglected without serious error to give the second term in Eq. 14 equal to

$$\frac{d - 2\ell}{C} - \frac{(d - 2\ell) v \cos \alpha}{C^2} \quad (18)$$

The first and third terms of Eq. 14 combine to yield  $\frac{2\ell}{C}$  and when this is added to the second term one gets

$$T_{1-2} = \frac{d}{C} - \frac{(d-2\ell) v \cos \alpha}{C^2} \quad (19)$$

The total phase shift between crystal  $X_2$  excitation voltage and the mechanically-induced signal voltage on crystal  $X_2$  from cross-coupled energy from crystal  $X_1$  is  $T_{1-2}$  divided by the period of the excitation frequency

$$\gamma - \theta = \frac{2 \pi f d}{C} - \frac{2 \pi f (d-2\ell) v \cos \alpha}{C^2} \quad (20)$$

and thus

$$\gamma = \frac{2 \pi f d}{C} \quad \theta = \frac{2 \pi f (d-2\ell) v \cos\alpha}{C^2} \quad (21)$$

The output voltage then becomes

$$e_s = 2 K_e K_s V \sin \frac{2 \pi f (d-2\ell) v \cos\alpha}{C^2} \sin\omega t + \frac{\omega d}{C} \quad (22)$$

The factor  $\omega d/C$  is related to probe dimensions and excitation frequency and therefore contributes no information regarding flow velocity. The function  $2 \pi f (d-2\ell) v \cos\alpha/C^2$  contains the useful information and produces amplitude modulation of the signal proportional to the sine of the function. For convenience let the following identity apply:

$$E = 2 K_e K_s \sin \frac{2 \pi f (d-2\ell) v \cos\alpha}{C^2} \quad (23)$$

Since  $d-2\ell = D/\sin\alpha$ , Eq. 23 becomes

$$E = 2 K_e K_s \sin \frac{2 \pi f D v \cot\alpha}{C^2} \quad (23a)$$

For a small value of velocity the phase shift produced is small, allowing  $\sin \theta$  to be replaced with  $\theta$ , and with  $\alpha = 45^\circ$  the ideal peak signal voltage is

$$E = \frac{4 \pi f K_e K_s V D v}{C^2} \quad (24)$$

For typical probes and probe-excitation voltages of 3 volts peak the value of  $K_e K_s V$  has been found to be nominally 0.5 volt. With  $f = 5$  MH and  $C = 1.55 \times 10^5$  cm per second, the theoretical signal level is then:

$$E = 13 D v \times 10^{-4} \text{ volts/cm}^2/\text{sec} \quad (25)$$

For flow measurement on a 1 centimeter internal diameter vessel, assuming velocities of 100 cm/sec, a 130 mv signal can be realized. This can be contrasted with an electromagnetic

level of 0.3 mv for the same position and a pickup signal on the order of several tens of microvolts for the back-scatter ultrasonic technique (Rushmer, 1966). The selection of the  $180^\circ$  quiescent phase difference between the pickup voltage results in excellent sensitivity. If the flow velocity exceeds the value which makes  $\theta = \pi/2$ , the flow velocity becomes indeterminate. In actuality, the flow velocity is quite low producing a phase shift of approximately 0.1 radians.

Negative flow can be detected by proper circuit manipulation. Proper adjustment of reactive balance circuits will produce an output signal at zero flow which increases with positive flow and decreases with reverse or negative flow. For the case of exact balance, the output signal as a function of flow velocity would appear as an absolute value. If the reactive balance is properly adjusted, the curve can be shifted to the left to produce an absolute value function with shifted axis. In this case, for zero velocity, the output has some positive value and increases for flow directed toward  $X_1$  to  $X_2$ , and decreases for flow directed from  $X_2$  toward  $X_1$ . A sufficiently large reverse flow will produce increasing outputs. This poses no great problem as the magnitude of reverse flow is typically small. Proper phase detection of the output signal can also be used to realize the ability to detect reverse flow. This is perhaps the desired technique as it does not require special care to insure that the system is in a proper operating region. For a bench system modern integrated circuits yield a simple means of detecting phase. However these circuits are not optimum for implant, and therefore systems employing strict phase shift techniques are not discussed in this chapter. The continuous operating mode is somewhat unstable and consumes excessive power and for these reasons is not optimal for implant. An optimum concept for implant appears to be a combination of pulsed operation for minimum power consumption and amplitude limitation for prevention of spurious amplitude variation from contaminating the flow signal. In this mode the crystals are pulsed in phase opposition for approximately 1 microsecond and measurements are conducted only on the received energy at each crystal. Appropriate gating and timing circuits are required to produce correct operation.

5. Flow Circuit. The circuit required to perform this operation as described is shown in Fig. 6. The output of a subcarrier oscillator is connected to the cathode gate of  $SCS_1$ . When the gate voltage rises above 0.7 volt,  $SCS_1$  turns on and forward biases the 5 mc oscillator transistor  $Q_3$  and

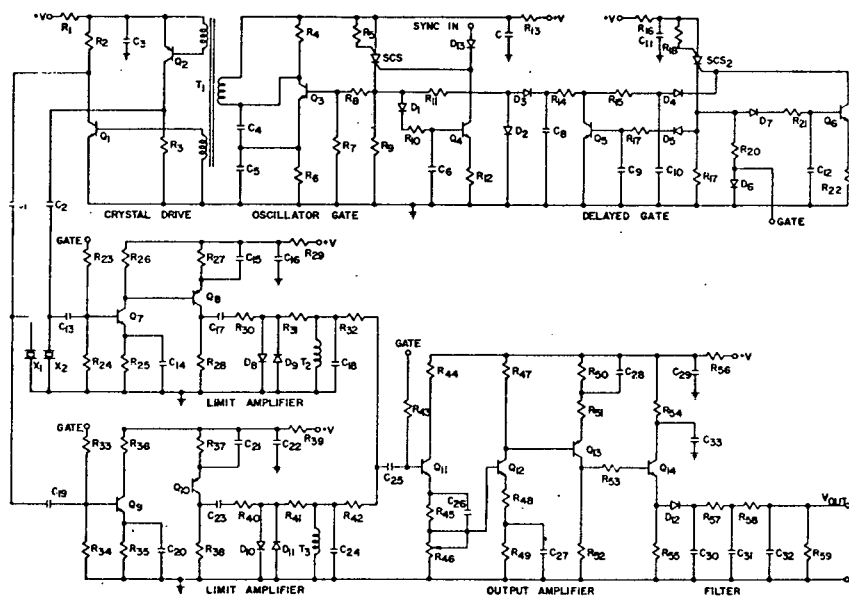


Figure 6. Blood Flow Signal Conditioner Schematic.

the 5 mc crystal driver amplifier transistors  $Q_1$  and  $Q_2$ . Coincidental with the  $SCS_1$  turn on, capacitor  $C_6$  starts to charge through  $R_{10}$ . When  $Q_4$  is sufficiently forward biased,  $SCS_1$  turns off. The pulse generated by  $SCS_1$  is limited by the series diode stack  $D_2$  and  $R_{11}$ . This constant amplitude pulse is deposited on  $C_8$  which in turn charges  $C_{10}$  through  $R_{14}$  and  $R_{15}$ , turning on  $SCS_2$ . The delayed pulse generated by  $SCS_2$  is then used to gate both limiting amplifiers and the output amplifier just prior to the arrival of the incident acoustical energy at each crystal.

The on time of the amplifiers is controlled by the time constant determined by  $R_{21}$  and  $C_{12}$ . The component network connected to the emitter of  $Q_{14}$  rectifies and filters the amplified RF signal, producing a DC signal proportional to flow velocity. The output is then connected to a subcarrier oscillator to produce frequency modulation proportional to flow velocity. The synchronization signal is also derived from the subcarrier oscillator.

For an ideal case where the crystals are well matched and the summing resistances are equal, the response curve is an absolute value function and reverse as well as forward flow appear as a positive voltage. A small capacitor placed in parallel with  $R_2$  or  $R_3$ , depending on the probe, results in improved measurement as the pickup signal on  $X_2$  then leads the pickup signal on  $X_1$ ; and thus for zero flow, there appears to be a flow from  $X_1$  toward  $X_2$ . Therefore at zero flow there is a positive voltage getting more positive for forward flow and less positive for reverse flow. Since the maximum negative flow is quite small, only a slight adjustment is required to acquire the ability to measure reverse flow.

#### D. Stability Consideration

Pressure stability is influenced by both biologic and electronic factors. Growth of tissue over the implanted transducer with consequent high velocity lateral flow can induce some error in pressure reading. Comparison of pressure measured by cannulation with that obtained by the transmitter yields an adequate calibration that incorporates both the tissue growth variable and the lateral flow variable.

The major stability problem is related to the long term drift of the transducer. Franklin et al. (1971), Konigsberg (1971), and Rader and Meehan (1971) have observed and reported long term drifts in these transducers. The initial work,



still incomplete, indicates that with premium transducers one may have a baseline drift of 6 mm Hg per month and a sensitivity drift of approximately  $\pm 3\%$  per month. The combination can then lead to a 12 mm Hg error over the period of a month. Temperature instability is not serious as the transducers have an output reasonably independent of temperature and also because the application is in a very narrow temperature range. So far a full appreciation of the long term drift is not available. At the moment the fact of the matter is that calibration after implant will be required periodically to confirm pressure readings. In implant application, if the long term drift is sufficiently small to prevent off-scale readings in the course of a year, one may well have to be content.

The flow device described suffers from two potential inaccuracies: one is purely electronic and therefore can be either fully eliminated or neutralized by compensation; the other stems from the inability to precisely measure the internal diameter of the vessel, and from the fact that the velocity profile is not blunt and in fact may be variable.

It is of some importance to realize that the output voltage is in terms of the product of blood flow velocity and the blood flow cross-sectional area. The quantity of flow can be calculated from

$$Q \left[ \frac{\text{cm}^3}{\text{sec}} \right] = \frac{\pi D^2 v}{4} \quad (26)$$

From an ideal theoretical consideration of the output signal and with amplification included after summation, it is possible to write the ideal peak voltage as

$$E = \frac{A_0 4 \pi f K_s K_e V D v \cot \alpha}{C^2} \quad (27)$$

A combination of Eqs. 26 and 27 yields an equation in which the quantity of flow is in terms of a measured voltage and several system parameters, some of which can be assumed to be constant. The flow is thus

$$Q = \frac{E C^2 D \tan \alpha}{16 f K_s K_e V A_0} \quad (28)$$

In general the only constants in the equation are the coefficients, the frequency  $f$ , and the gain  $A$ . The velocity  $C$  of ultrasound in tissue and body fluids varies with temperature, chemical constituents, and viscosity (Heuter and Bolt, 1955). The diameter  $D$  can be expected to vary with pressure, neural control, autoregulation, and mechanical events. The coupling coefficient  $K_s$  varies with the vessel wall thickness and the vessel contact, the chemical constituent of the conducting media, and the temperature and viscosity of the coupling media. The effective crystal drive voltage  $K_e V$  can be expected to vary with external components and with crystal loading which is influenced by the quality and temperature of the media.

For fixed environmental conditions it is possible to measure and assign fixed values to  $C$ ,  $D$ ,  $K_s$ , and  $K_e V$ . Due to improper knowledge of the precise values at this fixed environmental condition the resulting constant would likely be in error by  $\pm 10\%$ , as measurement of the diameter is probably only within  $\pm 5\%$  and other imprecise values contribute the additional  $5\%$ . With the assumption that the value of  $E$  can be measured very accurately, the calculated sensitivity inaccuracy is bounded by approximately  $\pm 10\%$ . The sensitivity inaccuracy associated with the back-scatter technique where the Doppler frequency is related to flow velocity (Franklin et al., 1964) by

$$F = \frac{2 F_e v \cos \alpha}{C}$$

(29)

cannot be less than approximately  $\pm 10\%$  if it is assumed that the diameter can again be measured to  $\pm 5\%$  and the parameters  $F_e$ , cosine  $\alpha$ , and  $C$  are determined exactly. Thus the interferometric technique appears to be at least an equivalent method in regard to absolute sensitivity at a given stable environmental condition.

An additional important question can be asked concerning the extent to which the sensitivity and the zero baseline will vary with the changing chemical and thermal environments. It has previously been developed that measurement stability is related to the properties of the crystals and their mounting structure; to the component stability of the electronics; and to the variation of velocity and attenuation of ultrasound in tissue and body fluids with temperature, pressure, and chemical composition. It is unlikely that the drive voltage on

each crystal would be equal in either phase or magnitude because of differences in mechanical loading; it is equally improbable that each crystal would respond equally to identical acoustical inputs because of unequal mechanical loading. For the continuous mode of operation the general equation for the sum of  $e_1$  and  $e_2$  can be written for magnitude and angle differences as:

$$\begin{aligned}
 e = & K_{e1} V_1 \cos (\omega t + \psi_1) - K_{e2} V_2 \cos (\omega t + \psi_2) \\
 & + K_{e1} K_{s2} V_1 \cos (\omega t + \gamma + \psi_{11} - \theta) \\
 & - K_{e2} K_{s1} V_2 \cos (\omega t + \gamma + \psi_{22} + \theta)
 \end{aligned}
 \tag{30}$$

Where  $K_{e1}$  and  $K_{e2}$  are related to the impedance of the crystals and the source,  $K_{s1}$  and  $K_{s2}$  are related to the attenuation factor of the media, to the quality factor of the crystals, and to the distance between crystals. The angles  $\psi_1$  and  $\psi_2$  are associated with the impedance of the crystals and source and  $\psi_{11}$  and  $\psi_{22}$  are angles associated with the mechanical response of the crystals to incident energy.

For purposes of analysis it is convenient to consider magnitude and phase imbalance separately and to consider the results as a worst case to obtain the maximum expected error. For magnitude consideration only, it is assumed that  $\psi_1 = \psi_2 = \psi_{11} = \psi_{22} = 0$ . This gives

$$\begin{aligned}
 e_s = & (K_{e1} V_1 - K_{e2} V_2) \cos \omega t \\
 & + K_{e1} K_{s2} V_1 \cos (\omega t + \gamma - \theta) \\
 & - K_{e2} K_{s1} V_2 \cos (\omega t + \gamma + \theta)
 \end{aligned}
 \tag{31}$$

The signal voltage  $e_s$  is the summation of four vectors, all of which are comparatively large and are variable with drive voltage, crystal and media properties, and component stability. Two of these vectors vary in phase with flow because of the flow-related term in their angle. The result of this angle variation is a nonlinear amplitude variation of the resultant signal voltage with flow. The first step toward eliminating this nonlinearity is to adjust  $V_2$  in Eq. 31 such that the first term is zero. If this is done with the condition imposed that  $\psi_1$ ,  $\psi_2$ ,  $\psi_{11}$ , and  $\psi_{22}$  equal zero, the equation simplifies to

$$e_s = \sqrt{[A_1^2 + A_2^2 - 2 A_1 A_2] + 4 A_1 A_2 \sin^2 \theta} \sin (\omega t + \phi) \quad (32)$$

where  $\phi$  is the angle of the composite vector and  $A_1 = V_1 K_{e1} K_{s2}$  and  $A_2 = V_2 K_{e2} K_{s1}$ . Thus only if  $A_1 = A_2 = A$  whence

$$e_s = (2A \sin \theta) \sin (\omega t + \gamma) \quad (33)$$

does one achieve a truly linear response with a small angle of  $\theta$ .

In Eq. 32 the first term in brackets under the radical produces a residual voltage related to the imbalance of  $A_1$  and  $A_2$  but unrelated to flow. The second term in brackets under the radical is the flow related term. Zero residual voltage is produced only if  $A_1 = A_2$ . The sensitivity is also directly proportional to the value of  $A_1$  and  $A_2$ . For variation of  $A_1$  and  $A_2$  around an arbitrary value of  $A$  by  $\pm 10\%$ , the residual voltage or zero baseline remains quite constant and close to zero. The sensitivity however varies by as much as 20%. A reciprocal change in  $A_1$  and  $A_2$  tends to stabilize the sensitivity, yet affects the zero stability very little. The linearity remains quite good throughout. Factors contributing to variance in  $A_1$  and  $A_2$  are drive voltage changes, crystal property changes, component value changes, and media property changes, all of which can be functions of time, temperature, and voltage.

In addition to its direct affect on the sensitivity by virtue of its influence on  $\theta$ , a change in frequency also affects all  $K$  values and thus  $A_1$  and  $A_2$ . The crystal response is similar to a resonant circuit and thus the  $K$  values are also dependent on frequency. Fortunately this can be precisely fixed by crystal-controlled oscillators. Sensitivity changes produced by velocity changes are squared and thus can contribute markedly to accuracy. The velocity is related to temperature, pressure, chemical concentration, density, and compressibility; thus one must be careful in assigning a constant to this parameter. Fortunately with most conditions velocity variation is quite small; for example, from water to blood the velocity change is about 3%, and the velocity variation in blood with temperature is about 0.3% per degree Centigrade and thus its affect on the output can be neglected for normal operation. The attenuation of the ultrasonic signal is also quite variable with temperature and also from

media to media. For a similar condition of temperature and distance, the signal received in the blood is about 75% of the corresponding condition in water. The change in attenuation of sound in water with temperature is negligible and in blood at approximate body temperature is about 2% per degree Centigrade. Since the output is directly proportional to the level of the cross-coupled signal without compensation one can expect a signal inseparable from flow of about 2% of full-scale per degree Centigrade.

Undesirable phase shift errors stemming from many of the same conditions that introduce magnitude-related errors also contribute to inaccuracies. For this analysis it is assumed that all magnitude differences have been nulled and the phase difference exists in the crystal excitation voltage due to off-resonance operation of each crystal and unequal phase shift properties of conditioning circuits.

With these simplifications the output signal becomes:

$$e_s = VK_e [\cos (\omega t + \psi_1) - \cos (\omega t + \psi_2)] \\ + K_e K_S V [\cos (\omega t + \gamma + \psi_{11} - \theta) - \cos (\omega t + \gamma + \psi_{22} + \theta)] \quad (34)$$

With no flow ( $\theta = 0$ ) two residual voltages exist because of angle imbalance due to out-of-phase drive and out-of-phase detection. This residual output is a function of all angles and only remains constant if the increment in  $\psi_1$  equals the increment in  $\psi_2$ , and the increment in  $\psi_{11}$  equals the increment in  $\psi_{22}$ . By adjustment of the input,  $\psi_1$  can be made equal to  $\psi_2$ ; and thus the first term cancels, leaving one residual voltage related to unequal phase shifts associated with the cross-coupled energy. For any particular condition the effects of these imbalances can be nulled; however, to obtain thermal and chemical stability, the value of  $\psi_{11}$  and  $\psi_{22}$  must track very closely. The value of all angles  $\psi_1$ ,  $\psi_2$ ,  $\psi_{11}$ , and  $\psi_{22}$  are related to frequency, temperature, chemical composition, and mechanical loading of the crystal. An analytical description of these angles is difficult to obtain, however, since the effect of this nontracking is a relative phase shift between the two crystal voltages; an experimental evaluation can be made by simply observing the phase shift as a function of the required condition. Such a test reveals that temperature-induced relative phase shift between crystal voltages is very small. However, the ultimate effect this change has is substantial because of the large common mode

excitation signal ( $VK_e$  in Eq. 34). The direction of this change is entirely a function of relative crystal properties.

Many of the inaccuracies associated with undesirable amplitude and phase changes induced by alterations in crystal properties and the attenuation properties of the conducting media can be reduced by proper conditioning of the signals derived from each crystal. The parameter  $K_e K_s V$  in Eq. 34 is not in reality a constant as it is dependent on both crystal and media properties. However this dependency can be reduced by limiting the signal voltage from each crystal prior to phase detection. The large common mode signal can be eliminated by pulsing the crystals.

The ultimate in stability at the cost of additional complexity but with considerable reduction in power consumption is achieved by a combination of pulse- and amplitude-limiting techniques. In this approach each crystal is excited for a brief period, usually about 1 microsecond, and measurement is conducted only on the cross-coupled energy to each opposite crystal. The signal from each crystal is after limiting.

$$e_1 = -\bar{V} \cos \omega t + \psi_1 + \theta$$

$$e_2 = \bar{V} \cos \omega t + \psi_2 - \theta$$

(35)

addition gives

$$e_s = \sqrt{2} \bar{V} \sqrt{1 - \cos(\psi_2 - \psi_1 - 2\theta)}$$

$$\theta = \frac{2 \pi f D v}{c^2}$$

(35a)

Common mode phases such as would occur due to changes in velocity of sound or probe dimensions and as represented by  $\psi$  do not affect the relative phase, and in this regard, do not affect the output signal. To the degree that these variables are contained within the function  $\theta$ , they do affect the measurement stability. From Eq. 35a it can be determined how variation in sound velocity, vessel diameter, and frequency affect the measurement stability. The variation in  $\bar{V}$  can be held to very small values, thus substantially reducing the dependency of the output voltage to random amplitude

variation. For practical applications it can be assumed that  $f$  is constant. Sound velocity in body fluids varies by approximately 0.6 meter/sec/C°, thus over a 10-degree span the velocity would increase by 600 cm/sec. On this basis, the error contributed by velocity variations due to temperature can be neglected. Velocity change associated with chemical composition is small, being on the order of 3% from pure water to blood, and this can possibly be neglected for the modest hematocrit changes that are to be expected.

The major error stems from a differential phase imbalance caused by resistive and reactive component value changes in the crystal with temperature and loading. As illustrated in Fig. 5, an electronic equivalent of each crystal is a series combination of resistance and reactance. To the effect of these components can be added the effect of the source impedance. The crystal components  $R_E$  and  $X_E$  vary with temperature, loading, and age. Generally both crystals tend to change in the same manner, but with unequal magnitudes, with the result that some residual phase change exists. For a well-defined temperature and loading condition which one expects in implant cases the differential phase change represented by  $\psi_1 - \psi_2$  is acceptably small, and the stability offered by this approach appears to be adequate.

It can be concluded from this analysis that for many experiments the accuracy and stability afforded by this measurement concept is adequate. It may also be concluded that it is at least as accurate as currently popular alternate concepts, while enjoying a significant circuit simplicity and a considerable advantage in power consumption.

#### E. Packaging Technique

Figure 7 illustrates a prototype package with a pressure sensor and a flow probe attached. Each amplifier, voltage regulator, power controller, and oscillator was assembled and potted, then interconnected within the package. The package was fabricated from cast acrylic and the cover was attached by stainless steel screws and sealed with an O-ring. The pressure sensor and flow probe were attached to the package by removable miniature connectors. Used with a 160 ma hour battery, the unit pictured will operate continually for approximately 80 hours. With the controller set to 4 minutes there is a potential of 1200 actuations. At an average of two recording events per day, an operating life of nearly two years is available. Shelf life of power supplies at the elevated temperature is likely to be a limiting condition.

Reproduced from  
best available copy.

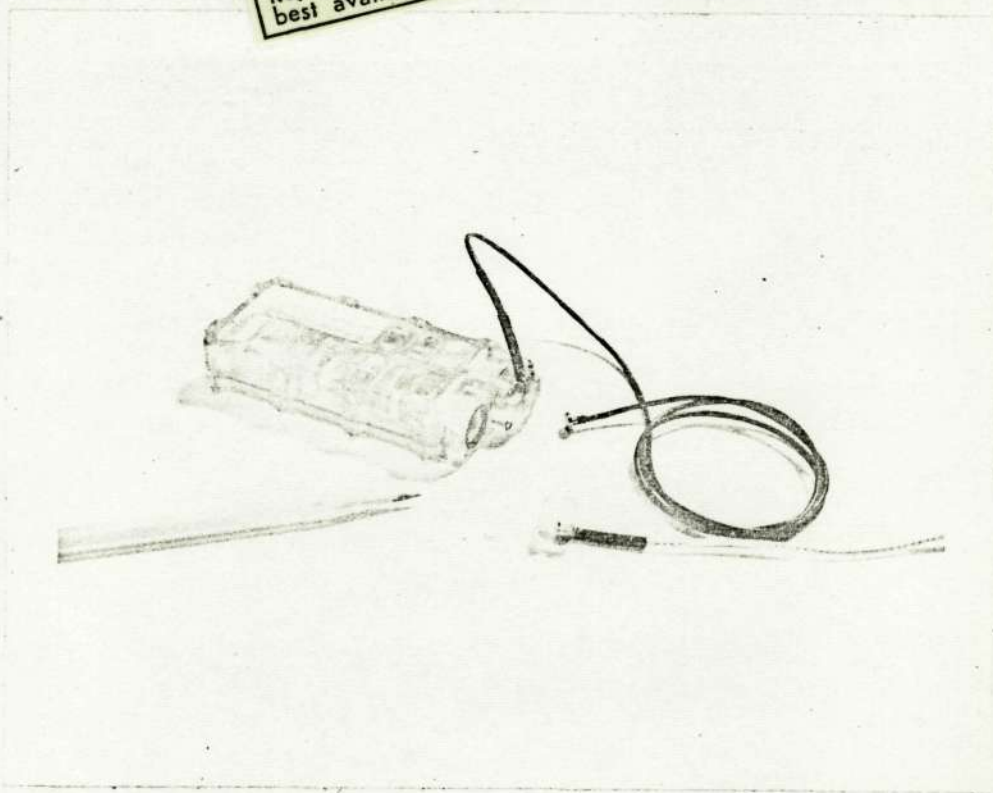


Figure 7. Implant Package with Pressure and Flow Sensors Shown.



Each module is assembled from a breadboard circuit by using cordwood techniques. The components are epoxied together, each making direct contact with adjacent components. Interconnection between components is made by a small gauge wire. Each module is then potted in a 16 x 10 x 12 mm volume. These modules are then interconnected as appropriate with required external components placed between the leads. The package sensor connections are brought to a bulkhead connector in the package and the sensors are mated to these bulkhead connectors by sealed plugs. Adjustment potentiometers are enclosed within the package. Prior to implant, exposed portions of the modules and the battery are covered with beeswax. This furnishes additional protection against leaks.

#### F. Evaluation

Testing this package and a similar prototype package has been accomplished during the past two years. There have been few problems associated with pressure measurement during this period, for an earlier program using the sensor and external electronics had eliminated most of them.

During this testing period, several problems associated with the flowmeter have been discovered and solved. Clearly, a rugged probe is necessary for structural and electronic stability and for consistency of calibration. The ultrasonic flow probe is a thick-walled acrylic tube with crystals placed at a 30-degree angle to the direction of flow. A slit in the tube allows the vessel to be placed between the crystals; the slit is closed by a press-fit slug. The leads to both crystals emanate from the cylinder tangentially to the circumference and opposite to the gate.

Implant technique is straightforward; it consists first of exposure of the renal and abdominal vessels via a longitudinal flank incision. The flow probe cavities are filled with gel foam, the probe is then placed about the renal vessel, and the small gate inserted to retain the vessel within the probe. The gel foam aids in tissue growth, shortening the grow-in time. The pressure sensor is inserted through a small incision in the abdominal aorta and sutured in place. A dacron patch encircling the entire vessel aids in anchoring the transducer. The package is sutured against the abdominal wall.

Pressure signals are of a high quality immediately postimplant; however, about four days are required for quality

flow signals to be received as a finite length of time is required for the flow probe to grow in. It has been found that fibrous tissue anchors the sensor and the package very firmly, and after two weeks, considerable effort is required to extract the equipment. To date an implant life of four months has been achieved.

Flow calibration is accomplished prior to implantation by placing the probe in a fixture and forcing known quantities of fluid through in varying times. The nominal sensitivity is 0.1 volt output per ml/sec. However, flow calibration can be conclusive only if it is actually carried out with the probe on the vessel. This is not easy but can be accomplished in the case of the kidney vessels by comparing the mean renal artery flow, as determined by the implanted probe and electronics, with a collection of the flow from the renal vein during the same period. A second technique, which can be conducted at the end of experimentation, is to cut the renal vessel and force fixed amounts of fluid through the vessel in a known time. This allows a fairly satisfactory calibration if air can be excluded from the blood that is being forced through the vessel. A combination of preimplant calibration, proper scaling for vessel diameter, and confirmation by either one or both of the in vivo techniques yields a calibration factor which is sufficiently accurate to be meaningful. Pressure calibration is also conducted prior to implantation by standard manometric techniques and periodically verified by cannulation techniques after implantation.

A variety of methods of affecting renal blood flow have been utilized in assessing the applicability of this implantable telemetry system for chronic studies. They have included psychosocial stressors, pharmacological agents, and treadmill exercise. An exercise episode will suffice to illustrate the application of the device and to substantiate its utility. Before exercise, an implanted dog was held in the obedience training "stand-stay" position on the treadmill for 3 minutes. Exercise consisted of running on a 15-degree incline for 3 minutes each at 2 and 3 miles per hour, and for 5 minutes at 4.5 miles per hour; then back to 2 miles per hour for 3 minutes, followed by 3 minutes of "stand-stay" on the treadmill. Typical results are illustrated in Fig. 8. For this dog mean pressure fell at the onset of exercise with perhaps a slight increase in mean blood flow. Pulse pressure fell while pulse flow increased. Throughout the course of the exercise mean pressure increased and mean flow decreased, while pulse pressure remained substantially unchanged and pulse flow increased.

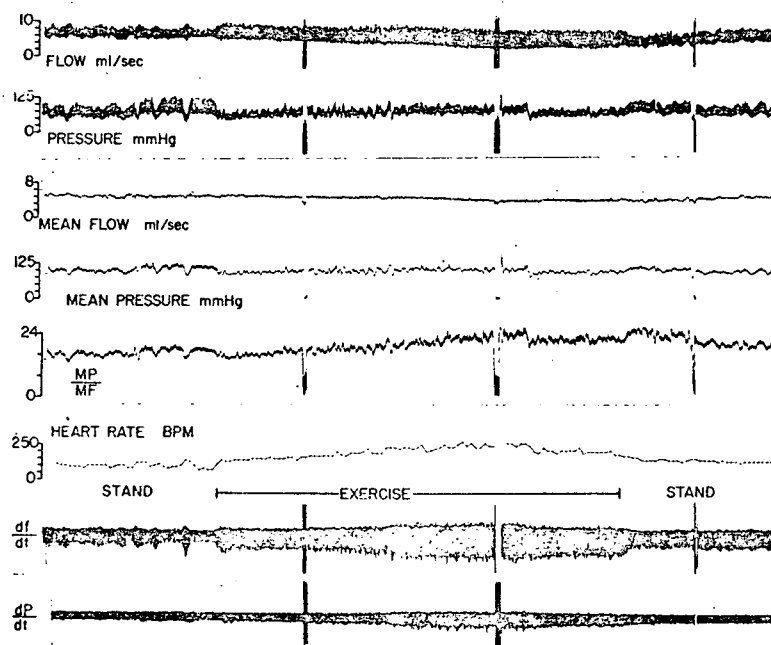


Figure 8. Data Obtained from an Exercise Event. An instrumented dog was exercised on a treadmill inclined at 15 degrees sequentially at speeds of 2, 3, 4.5, and 2 mph for respective periods of 3, 3, 5, and 3 minutes. Three-minute control periods preceded and followed exercise. From taped dynamic pressure and flow, mean pressure and flow were electronically calculated and the absolute resistance to flow determined by electronically dividing mean pressure by mean flow. The time rate of pressure and flow change was electronically generated to aid in analysis of the hydraulic impedance. One apparent conclusion is that at the start of exercise mean renal flow remained constant as a consequence of vasodilatation but throughout exercise decreased because of vasoconstriction. The increase in  $df/dt$  postexercise relative to preexercise indicates an increasing system compliance.

Since mean flow decreased and mean pressure increased, the absolute value of the resistance to flow increased. Also at the onset of exercise,  $df/dt$  increased and  $dp/dt$  remained constant; while throughout exercise, both  $df/dt$  and  $dp/dt$  increased. At cessation of exercise, mean blood pressure increased, mean flow remained at the lower level established during exercise, and the pulse flow returned to a level above that at preexercise. The rate of flow change  $df/dt$  and the rate of pressure change  $dp/dt$  both returned to substantially the same level existing at preexercise. From these observations certain conclusions can be made and certain evidence gathered supporting cortical-to-medullary flow shifts. These results indicate a definite decrease in resistance to renal blood flow at the beginning of exercise, followed by an increase in resistance as exercise continues. This renal blood flow pattern would seem to correlate with the recent work of Stinson *et al.* (1969) who have demonstrated cholinergic vasodilatation during the reduction of mean renal arterial pressure. It can further be noted that probably, as a function of the severity of exercise and the concomitant increase in oxygen consumption of the exercising muscles, there is an increased resistance to renal blood flow, an increased heart rate, and an increased mean blood pressure--all of which reflect increased metabolic demands (Krutz *et al.*, 1971).

Evidence for the cortical-to-medullary flow shift can be gathered by considering the characteristics of the flow throughout the exercise episode. For a rough approximation, flow to the kidney (Spencer and Denison, 1963) can be defined by

$$f = C \frac{dp}{dt} + \frac{p}{R} \quad (36)$$

where  $f$  is flow in ml/sec,  $p$  is pressure in dynes/cm<sup>2</sup>;  $C$  is compliance defined by  $2\pi r^3/Et$ \*;  $r$  is the vessel radius;  $t$  is vessel wall thickness;  $\ell$  the segment length; and  $E$  the modulus of elasticity;  $R$  is resistance defined by  $8\eta\ell/\pi r^4$ , where  $\eta$  is the blood viscosity. The factor  $df/dt$  is thus defined by

$$\frac{df}{dt} = C \frac{d^2 p}{dt^2} + \frac{1}{R} \frac{dp}{dt} \quad (37)$$

---

\*It may be that compliance is defined by  $\frac{2 \pi r^3 \ell}{Et}$

On the basis of Eq. 36, at the onset of exercise since there was a decrease in systolic pressure, but initially no change in maximum  $dp/dt$ , yet there was an increase in maximum flow and a decrease in minimum flow, it would appear that C increased and R remained unchanged; or R decreased and C remained unchanged; or both C increased and R decreased. Comparison of a term labeled systolic resistance determined during systole where  $dp/dt$  is zero illustrates that the resistance has decreased from its preexercise value. And since C is also proportional to the radius  $r$ , it would seem probable that the compliance has also increased.

One can also argue that at the onset of exercise, the increase in  $df/dt$  described by Eq. 37 is a consequence of decreasing resistance and increasing compliance as  $dp/dt$  did not increase. A decrease in resistance and consequently an increase in the effective flow radius can be confirmed by considering points where  $dp/dt$  is zero, where the first term in Eq. 36 is zero. Resistance determined at this point on the cardiac cycle by dividing the pressure by the flow yields a lower value shortly after start of exercise than for corresponding points determined during preexercise; and by considering Eq. 36, during a very short section of systole where the change in pressure is small, but the rate of pressure change is large, an estimate of the compliance value can be made. The first term in the equation is then closely related to the delta flow. This term is a product of the compliance and the rate of pressure change; thus if  $dp/dt$  does not change from preexercise to shortly after exercise, but the pulse flow increases, it must be argued that the compliance increased. Figure 8 illustrates that  $dp/dt$  did not increase in the transition from "stand-stay" to exercise, but the pulse flow did increase. The compliance therefore must have increased.

As exercise continues, the mean resistance increases which implies decreasing radius and therefore a decreasing compliance; yet the pulse flow remains high or increases relative to preexercise values. These observations must be considered in light of the fact that  $dp/dt$  also increases during this period. Equations 36 and 37 indicate that the character of the flow is influenced to a substantial degree by  $dp/dt$ . Thus the direction of capacitance from shortly post-exercise to near completion of exercise cannot be reliably deduced without an extensive analysis of magnitudes.

Postexercise, the mean flow is definitely down relative to the start of exercise in the face of a relatively elevated

pressure level. Pulse flow has decreased to slightly above preexercise levels and slightly below onset of exercise levels. The resistance value as judged by the minimum flow level has certainly increased from preexercise, allowing a conclusion that the effective radius has decreased. At post-exercise peak  $dp/dt$  has returned to its preexercise value, but the capacitive component of flow determined at onset of systole is as large or larger than preexercise values. This would lead to the conclusion that the compliance has increased or at least remained unchanged over preexercise levels. But how can this be if the effective radius has decreased? Consideration of Eq. 37 tends to confirm this conclusion. The rate of change of flow postexercise is greater than that at preexercise, but the value of the resistance has increased, and the level of  $dp/dt$  pre- and postexercise is nearly equal. This means that the second term in Eq. 37 is smaller during postexercise cardiac cycles than during preexercise cycles. Therefore if  $df/dt$  at pre- and postexercise is equal, then the downward increment induced by an increasing resistance has to be nullified and overcome by an upward increment in the compliant flow term. If  $dp/dt$  has not increased, then compliance must have increased relative to its preexercise value. A decrease in effective flow area through the kidney without a concomitant decrease in compliance appears inconsistent with traditional concepts of hemodynamic impedances. But it could occur if flow shifted from many cortical vessels to fewer, larger-diameter, more compliant vessels in the medullary area of the kidney.

It is appreciated that the arguments presented in support of theories suggesting a shift from cortical to medullary flow are circumstantial. Direct evidence is necessary to support these contentions. However this argument has been presented as an example of an application of telemetry and to justify our removing it from a device still in the developmental stage to one having useful applications. Indeed because of the role the kidney plays in fluid volume regulation it can be argued that the research application of telemetry of the type just described is quite valuable in orbital animal experiments. If direct evidence can be obtained to support the impedance concepts presented above, then one has a valuable indirect measurement of renal responses which could be applied to research in renal function in unrestrained subjects.

## G. Circuit Values

Circuit values are tabulated in this section to aid those who may wish to fabricate portions of the described telemetry system. Generally, 5% resistor and 10% capacitor values have been employed; thus the listed values should be used principally as a guide. These components which are likely to need further adjustments are noted with an asterisk.

### Carrier Oscillator (Fig. 1)

(Capacitance in pf; resistance in  $K\Omega$  ; inductance in  $\mu h$  unless otherwise noted)

R5 - 270	C4 - 33
R6 - 8.2	C5 - 33
R7 - 3.9	L1 - 5.5t #18 copper wire 3/16 dia
R8 - 1.5	RFC1 - WE-WE minaductor 0.82 $\mu h$
C2 - 1.5 $\mu f$	RFC2 - WE-We minaductor 0.82 $\mu h$
C3 - 7	Q3 - 2N 918.

### Blood Flow - Subcarrier Oscillator (2300 H2) (Fig. 2)

(Capacitance in pf; resistance in  $K\Omega$  ; inductance in  $\mu h$  unless otherwise noted)

R1 - 330	R11 - 390
R2 - 220	R12 - 24
R3 - 220	C1 - 300
R4 - 220	C2 - 300
R5 - 220	C3 - 300
R6 - omit	C4 - 300
R7 - 390	C5 - 1000
*R8 - 51	C6 - 1 $\mu f$
R9 - 8.2	C7 - 2200
*R10 - 68	Q1/Q2 - SP8888A - dual flat pack

---

\*Adjust limit frequencies by varying R<sub>8</sub> and R<sub>10</sub>.

R.F. Switch (Fig. 3)

(Capacitance in pf; resistance in  $K\Omega$  ; inductance in  $\mu h$  unless otherwise noted)

R1 - 270	R10 - 560	C4 - 100
R2 - 5.1	R11 - 51	C5 - 15 $\mu f$
R3 - 7.5	R12 - 2.4	C6 - 0.02
R4 - 5.1	R13 - 390	D1 - D6 - FDN666
R5 - 1000	R14 - 0.1	SCS1 - 3N84
R6 - 51	R15 - 0.1	SCS2 - 3N84
R7 - 430	C1 - 1000	Q1/Q2 - MD6001F
R8 - 200	C2 - 470	Q3/Q4 - SP8888A
R9 - 6 meg	C3 - 300	L10 Pancake coil wound to Co resonate at desired frequency (approx. 500 KH)

Blood Pressure with Oscillator (3900 H2) (Fig. 4)

(Capacitance in pf; resistance in  $K\Omega$  ; inductance in  $\mu h$  unless otherwise noted)

R1 - omit	R18 - 220	C5 - 2200
R2 - 0.047	R19 - 220	C6 - 0.022 $\mu f$
R3 - 30	R20 - 51	C7 - 0.33 $\mu f$
R4 - 3	R21 - 220	C8 - 180
R5 - 5.6	R22 - 4.7	C9 - 560
R6 - 15	R23 - 220	C10 - 180
R7 - 0.091	R24 - 62	C11 - 1 $\mu f$
R8 - 0.2	R25 - 220	C12 - 180
R9 - 2	R26 - 220	C13 - 1500
R10 - 2	R27 - 24	C14 - 180
R11 - 220	R28 - 220	C15 - 0.01 $\mu f$
R12 - 220		D1 - D5 - FDN666
R13 - 0.2		SCS1 - 3N82
R14 - 2	C1 - 1000	Q1/Q2 - MD2219 - dual flat pack
R15 - 2	C2 - 2200	Q3/Q4 - MD2904 - dual flat pack
R16 - 220	C3 - 0.022 $\mu f$	Q5/Q6 - SP8888A - dual flat pack
R17 - 200	C4 - 0.33 $\mu f$	

Resistor  $R_C$  controls sensor drive current, resistors  $R_{12}$  and  $R_{17}$  control modulation sensitivity and resistors  $R_{20}$  and  $R_{24}$  control limit frequencies.



Blood Flow without Oscillator (Fig. 6)

(Capitance in pf; resistance in K $\Omega$  ; inductance in  $\mu$ h, unless otherwise noted)

R1 - 0.1	R33 - 9.1	C5 - 1000
R2 - 0.18	R34 - 10	C6 - 470
R3 - 0.18	R35 - 0.100	C7 - 15 $\mu$ f
R4 - omit	R36 - 0.510	C8 - 1000
R5 - 51	R37 - 0.100	C9 - 330
R6 - 220 $\Omega$	R38 - 0.510	C10 - 180
R7 - 2.4	R39 - 0.100	C11 - 15 $\mu$ f
R8 - 1.5	R40 - 0.100	C12 - 560
R9 - 2.4	R41 - 1.2	C13 - 47
R10 - 15	R42 - 2.4	C14 - 180
R11 - 0.510	R43 - 15	C15 - 1800
R12 - 0.510	R44 - short	C16 - 15 $\mu$ f
R13 - 0.100	R45 - 0.056	C17 - 150
R14 - 2.4	R46 - 0.500	C18 - 47
R15 - 20 K	R47 - 0.560	C19 - 47
R16 - 0.100	R48 - 0.051	C20 - 180
R17 - 24	R49 - 0.056	C21 - 1800
R18 - 51	R50 - 0.051	C22 - 15 $\mu$ f
R19 - 1.5	R51 - 0.051	C23 - 150
R20 - 1.2	R52 - 0.560	C24 - 47
R21 - 27	R53 - 0.150	C25 - 22
R22 - 0.110	R54 - 0.100	C26 - 2700
R23 - 9.1	R55 - 1	C27 - 330
R24 - 10	R56 - 0.100	C28 - 3300
R25 - 0.100	R57 - 10	C29 - 15 $\mu$ f
R26 - 0.510	R58 - 10	C30 - 3300
R27 - 0.100	R59 - 330	C31 - 4700
R28 - 0.510	C1 - 0.02 $\mu$ f	C32 - 0.1 $\mu$ f
R29 - 0.100	C2 - 0.02 $\mu$ f	C33 - 15 $\mu$ f
R30	C3 - 15 $\mu$ f	D1-D18 - FDN666
R31 - 1.2	C4 - 100	SCS1 & SCS2 - 3N84
R32 - 2.4		

---

All NPN transistors are MPS 6515 and PNP MPS 6519.

H. References (Section II - Development of an Implantable Telemetric Data Acquisition System)

Brown, J. H. U., Jacobs, J. E., and Stark, L. (1971). Bio-medical Engineering. F. A. Davis Co., Philadelphia.

Caceres, C. A. (1965). Biomedical Telemetry. Academic Press, New York.

Franklin, D. L., Watson, N. W., and Van Citters, R. L. (1964). "Blood Velocity Telemetered from Untethered Animals." Nature 203 (4944):528-530 (Aug. 1).

Franklin, D., Patrick, T., Kemper, S., and Vatner, S. (1971). "A System for Radiotelemetry of Blood Pressure, Blood Flow and Ventricular Dimensions from Animals - A Summary Report." Proc 1971 Int Telemetering Conf, Washington, D.C., Sept. 27-29, 7:244-250.

Fryer, T. B. (1970). Implantable Biotelemetry Systems." Proc 1970 Natl Telemetering Conf, Los Angeles, April 27-30, pp. 91-96.

Heueter, T. F. and Bolt, R. H. (1955). Sonics. Techniques for the Use of Sound and Ultrasound in Engineering and Science. John Wiley & Sons, Inc., New York.

Konigsberg, E. (1966). A Pressure Transducer for Chronic Intravascular Implantation. Presented at the 4th National Biomedical Sciences Instrumentation Symposium, Anaheim, Calif. (May).

Konigsberg, E. (1971). Personal communication.

Krutz, R. W., Rader, R. D., Meehan, J. P., and Henry, J. P. (1971). "Applicability of Implantable Telemetry Systems in Cardiovascular Research." Proc 1971 Int Telemetering Conf, Washington, D.C., Sept. 27-29, 7:239-243.

Landee, R. W., Davis, D. C., and Albrecht, A. P. (1957). Electronic Designer's Handbook, McGraw-Hill, Inc., New York.

Plass, K. G. (1964). "A New Ultrasonic Flowmeter for Intravascular Application." IEEE Trans Biomed Eng 11(4):154-156 (Oct.).

- Rader, R. and Griswold, K. (1965). "Carrier and Subcarrier Oscillations for Implanted Transmitters." Proc 18th Annual Conf Engin Med Biol, Philadelphia.
- Rader, R., Sears, W. J., Reid, D. H., Meehan, J. P., and Henry, J. P. (1967). "Transmission of Direct Blood Pressure from Dogs during Obedience Training." Proc 1967 Int Telemetering Conf, Washington, D.C., Oct. 2-4, 3:307.
- Rader, R., Meehan, J. P., Henry, J. P., Krutz, R., and Trumbo, R. (1968). "Transmission of Cardiovascular Data from Dogs." Proc 1968 Int Telemetering Conf, Los Angeles, Oct. 8-11, 4:597.
- Rader, R. D. (1971). "Cardiovascular Telemetry Implants." Telemetry J 6(3):15-20 (April/May).
- Rader, R. D. and Meehan, J. P. (1971). Observation of Arterial Blood Pressure of the Primate. (Unpublished NASA Report for Contract No. NSR 050018-07 for the period June 1-August 31, 1971).
- Rushmer, R. F. (1966). Methods in Medical Research. Vol. 2, Year Book Medical Publishers, Chicago.
- Sears, W. J. (1968). Telemetered Blood Pressure and Heart Rate in Dogs during Graded Treadmill Exercise, Natural Activity and Situational Stress. Ph.D. dissertation, University of Southern California, Los Angeles. (Physiology)
- Spencer, M. P. and Denison, A. J. Jr. (1963). "Pulsatile Blood Flow in the Vascular System." In Handbook of Physiology, Section 2; Circulation, Vol. II (W. F. Hamilton, ed.) American Physiological Society, Washington, D. C., Chap. 25, pp. 839-864.
- Stinson, J. M., Barnes, A. B., Zakheim, R. M., Chimoskey, J. E., Spinelli, F. R., and Barger, A. C. (1969). "Reflex Cholinergic Vasodilatation during Renal Artery Constriction in the Unanesthetized Dog," Amer J Physiol 217(1):239-246 (July).

NASA Contract Number

NSR 05-018-087

III. Cardiovascular Research Applications

- A. Introduction
- B. Renal Hemodynamic Model
- C. Experimental Application in Renal Function
- D. Pitfalls and Problems
- E. Discussion
- F. References

IV. Conclusions

### III. Cardiovascular Research Applications

#### A. Introduction

The sympathoadrenal system complex is responsive to a variety of psychological and physiological factors which via alterations in renal impedance cause variations in fluid and electrolyte balance. Thus superimposed upon the autoregulatory phenomenon in the kidney lies a rapidly acting neural-endocrine control mechanism which also influences renal functions. In much of the renal research in the past plasma clearance techniques have been used to measure renal parameters, such as renal blood flow and glomerular filtration rate. This technique is employed routinely in current renal research. Because of the nature of the measurement the results are an average value, the data is obtained during restraint and/or anesthesia, and the segmental renal resistances and compliances can not be determined. Within the past decade, research in renal circulation has benefited from the ability to measure dynamic flows and pressures. Analysis of this data has typically considered mean flow and pressure as a means of assessing renal responses to selected stimuli.

Recent work with simultaneous pressure and flow measurements in dogs has shown that wave shapes and amplitudes can be used to estimate values of these renal vascular compliances and resistances. This technique permits the total renal resistance to be separated in pre- and postglomerular components and the renal artery compliance to be determined. From the pre- and postglomerular resistance values the glomerular filtration pressure can be estimated. It is believed that these relationships provide an indicator of change in renal hemodynamics which is more revealing than either mean pressure and flow responses or the plasma clearance measurements. In both the renal and the general circulation resistance and compliance values affect short term control of blood pressure and the long term control of both fluids and electrolyte balance and blood pressure. On a short term basis neurostimulation results in elevation of blood pressure because of a general vasoconstriction of the vascular system. Chronic neurostimulation leads to a thickening vascular wall and to a reduction in lumen diameter and potentiation of the smooth muscle response to sympathetic stimulation. Also tissue nutrition may be impaired by high systemic blood pressure because of sclerotic development in the small arteries. In this case, sclerotic development may be exacerbated by local regulatory mechanisms which call for an increased pressure to

overcome the nutritional impairment evoked by sclerotic development (Henry and Meehan, 1971). The renal system can be implicated as a factor in many cases of hypertension. However it is difficult to say if it is a primary factor in inducing hypertension through the renin-angiotensin-aldosterone loop or a secondary factor evolving from impairment induced by sclerosis and smooth muscle potentiation.

The application of implanted telemetry for chronically monitoring systemic blood pressure and renal flow permits quantification of hemodynamic components of the renal vascular bed in unrestrained dogs which may aid in establishing the genesis of hypertension. It is suggested that these component values can be used as indices of renal function, levels of autonomic arousal, level and location of renal atherosclerosis, and further because of the apparently differing effects neurogenic and hormonal influences have on the component values, i.e., there are indications that control of preglomerular resistance is both hormonal and neural whereas control of postglomerular resistance is primarily hormonal, an assessment of the relative contribution of the neurogenic hormonal factors operating in a given situation may be made.

#### B. Renal Hemodynamic Model

Blood flow in the kidney is through multiple individual channels branching from the interlobular artery. These channels are similar in anatomical arrangement but vary in diameter, in length, and in the relative amount of collagen and elastin. In each channel the first major resistance site is encountered at the afferent arteriole vessel which branches from the interlobular artery and opens into the glomerular capillary. This capillary has a large surface area and behaves hydraulically as a large diameter storage volume and stores a large volume at a low pressure. On the exit side of the glomerular capillary but prior to the peritubular capillary, the efferent arteriole in parallel with the effective tubular resistance forms the second major resistive site. Downstream from the compliant peritubular capillary, a third resistive area is encountered. From this third resistive site the flow channels join the interlobular vein. The renal artery with its smaller branching supply vessels and the renal vein with its associated smaller connecting vessels add a resistance and a compliance which precede and follow all the elements created by the multiple parallel flow channels. Figure 9 illustrates a proposed hydraulic equivalent of one flow channel originating at the interlobular artery and terminating

in the interlobular vein (Rader et al., 1972). In terms of the pressure at the afferent arteriole and the pressure in the glomerular capillary, the flow through one of the many afferent arterioles and into one of the many compliant elements is respectively:

$$\begin{aligned} f_{ar} &= \frac{P_i - P_g'}{R_a'} \\ f_{ac} &= C_i' \dot{P}_i^* \end{aligned} \quad (1)$$

where  $\dot{P}_i$  is the first time differentiation of  $P_i$ . The sum of "n" of these individual flows where it is assumed that  $P_g'$  and  $R_a'$  and  $C_i'$  are equal to their respective counterparts in each individual flow channel is:

$$f_{a1} + f_{a2} + f_{a3} \dots + f_{an} = n C_i' \dot{P}_i + \frac{P_i - P_g'}{R_a'/n} \quad (2)$$

Also since in each channel the flow through  $R_a'$  must equal the compliant and resistive outflow at the node where  $R_a'$  joins  $C'g$ , it can be stated that:

$$\frac{P_i - P_g'}{R_a'} = C_g' \dot{P}_g' + \frac{P_g' - P_p'}{R't} \quad (3)$$

where  $R't$  is a composite of  $R'e$ ,  $R'g$  and  $R'p$ . The total flow in one kidney is the sum of flow in all channels.

If there are "n" identical channels it follows that:

$$\frac{P_i - P_g'}{R_a'/n} = n C'g \dot{P}'g + \frac{P'g - P'p}{R't/n} \quad (4)$$

Equations 1 through 4 substantiate that the many parallel flowpaths can be combined into a single flowpath where each discrete resistance is divided by and each compliance is

---

\*Compliance is defined as change in volume Q per change in pressure P. Thus  $C = dQ/dP$ . Manipulation and division by dt gives  $C \frac{dP}{dt} = \frac{dQ}{dt}$ ; but  $dQ/dt$  is flow f, therefore  $f = C \frac{dP}{dt}$ .

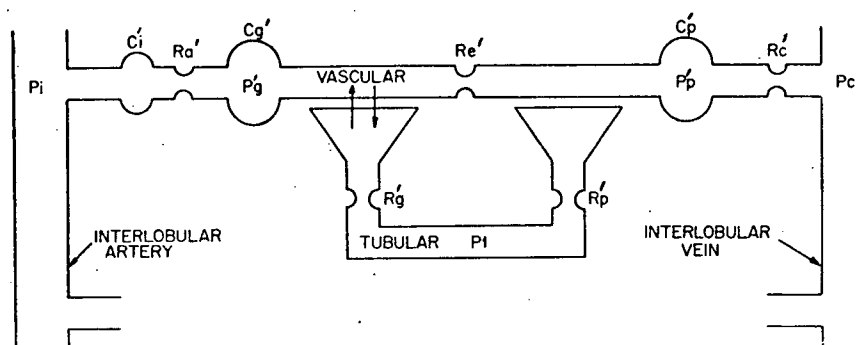


Figure 9. Hydraulic representation of a kidney. Flow is through multiple channels of similar structure. P's are pressures in mm Hg; C's are compliance in ml/mm Hg; R's are resistances in mm Hg/ml/sec.

C'i is the individual compliance in each arteriolar vessel.

R'a is the individual afferent resistance.

C'g is the individual glomerular capillary compliance.

R'e is the individual efferent arteriolar resistance.

R'g is the individual filtration resistance.

R'p is the individual absorption resistance.

C'p is the individual peritubular capillary compliance.

R'c is the individual postcapillary resistance.



multiplied by the number of parallel paths. An electronic model of an ideal kidney is illustrated at the top right in Fig. 10. The component values illustrated represent composites of all individual component values in each flowpath. The resistance offered by the larger supply arteries and collecting veins is thought to be small in comparison to the afferent arteriolar resistance and for a first approximation are neglected. The compliance contained in the renal artery and smaller arterial supply vessels is lumped with the compliance represented by  $C_i$ . In the present model, mass of blood in the renal supply vessels is also neglected and it is assumed that the resistance and compliance does not vary with pressure.

Flow into this model is then the sum of the flow into the storage element preceding the afferent arteriole and of that through all the afferent arterioles. This can be formulated as:

$$f = C_i \dot{P}_i + \frac{P_i - P_g}{R_a} \quad (5)$$

where  $\dot{P}_i$  is the first time differential of  $P_i$ . The character of the instantaneous pressure,  $P_i$ , the time rate of pressure change  $\dot{P}_i$  and the instantaneous flow  $f$  are illustrated on the left in Fig. 10. The first differential of Eq. 5 yields:

$$\dot{f} = C_i \ddot{P}_i + \frac{\dot{P}_i}{R_a} - \frac{\dot{P}_g}{R_a} \quad (6)$$

where the double dot indicates the second time differential. The time rate of flow change  $\dot{f}$  is illustrated at the bottom left in Fig. 10. In the bottom right of Fig. 10 salient points of the model development are summarized. Because of the buffering effect of the large glomerular compliance in series with the afferent arteriolar resistance, the factor  $\dot{P}_g/R_a$  may be neglected for steep incremental pressure changes in  $P_i$ . On the basis of a comparative cross-sectional area listed by Thompson (1970) it is probable that the glomerular compliance is on the order of 100 times the supply vessel compliance. The value of the supply vessel compliance has been estimated as nominally 0.002 ml/mm Hg. The afferent arteriolar resistance is nominally 10 mm Hg/ml/sec, and at 1 Hz the glomerular capillary reactance is approximately 0.8 mm Hg/ml/sec; hence, the assumption that  $\frac{\dot{P}_g}{R_a}$  is negligible for high frequency components appears valid. Therefore during

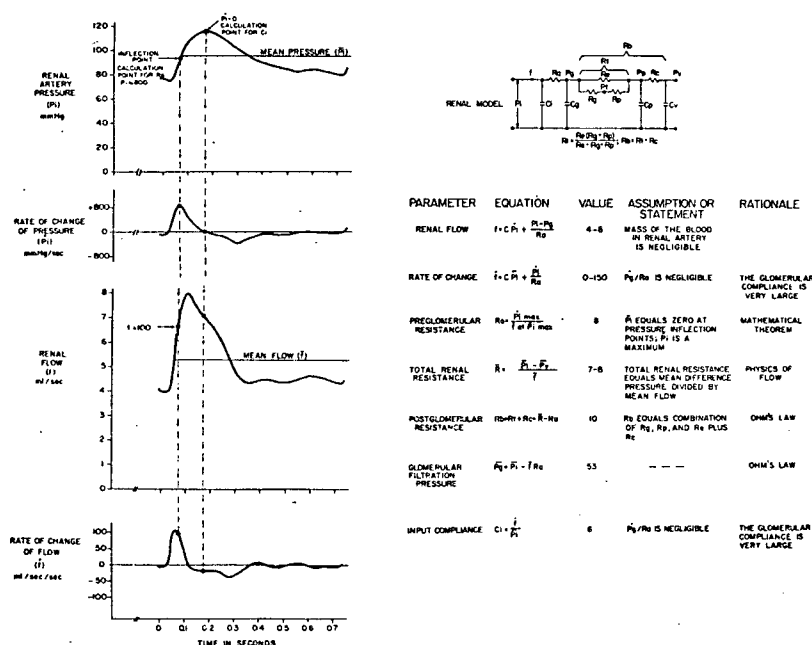


Figure 10. Renal parameter estimation technique. The renal model is illustrated at the top right, wave shape are illustrated on the left and the bottom right tabulates the equation and presents assumption and rationale.

rapidly changing small segments of input pressure, where  $\dot{P}_g$  can be assumed to be negligible, the following equation results:

$$\dot{f} = C \ddot{P}_i + \frac{\dot{P}_i}{R_a} \quad (7)$$

At the inflection point on the systolic portion of the input pressure, marked by the left hand dashed line in Fig. 10,  $\dot{P}_i$  is a positive maximum and  $\ddot{P}_i$  is therefore zero. Thus the afferent arteriolar resistance  $R_a$  can be calculated by dividing the value of  $\dot{P}_i$  by the value of  $\dot{f}$  at the inflection point. Therefore:

$$R_a = \frac{\dot{P}_i}{\dot{f}} \quad (8)$$

Equation 8 yields an estimate of the effective resistance preceding the glomeruli. This resistance is considered to be principally embodied in the afferent arterioles but, as previously mentioned, a small portion is also associated with the renal connecting vessels.

The mean flow for one cycle as defined by  $\bar{f}$  is:

$$\bar{f} = \frac{1}{T_2 - T_1} \left[ \int_{T_1}^{T_2} C_i \dot{P}_i dt + \int_{T_1}^{T_2} \frac{(P_i - P_g)}{R_a} dt \right] \quad (9)$$

where  $T_1$  is time at the start and  $T_2$  the time at the end of a cycle. Assuming that the pressure at  $T_1$  equals the pressure at  $T_2$ , the contribution of the compliant element vanishes.\*

---


$$\int_{T_1}^{*T_2} C_i \dot{P}(t) dt = C_i P(T_2) - C_i P(T_1) \text{ but } P(T_1) = P(T_2)$$

$$\therefore \int_{T_1}^{T_2} C_i \dot{P}(t) dt = 0$$

With proper substitution Eq. 9 can be simplified to:

$$\bar{f} = \frac{1}{R_a + R_t + R_c} \frac{1}{T_2 - T_1} \int_{T_1}^{T_2} (P_i - P_v) dt \quad (10)$$

The mean resistance  $\bar{R}$  is defined by the mean pressure gradient across the kidney divided by mean flow. Mean pressure across the kidney is the bracketed portion of Eq. 11. Performing the integration yields

$$\bar{R} = \frac{\bar{P}_i - \bar{P}_v}{\bar{f}} = R_a + R_t + R_c \quad (11)$$

where  $R_a$  is the preglomerular resistance,  $R_t$  is the composite of the filtration resistance  $R_g$ , the absorption resistance  $R_p$  and the efferent arteriolar resistance  $R_c$  and where  $R_c$  is the postperitubular capillary resistance. Therefore by dividing mean difference pressure across the kidney by mean flow one obtains the sum of the three resistance values. The combination of Eqs. 8 and 11 yields a value for the postglomerular resistance  $R_b$  of:

$$R_b = R_c + R_t = \frac{\bar{P}_i - \bar{P}_v}{\bar{f}} - \frac{\dot{P}_i}{\dot{f}} \quad (12)$$

The mean value of the glomerular capillary pressure  $\bar{P}_g$  is a function of these resistances and pressures as follows:

$$\bar{P}_g = \frac{\bar{P}_i R_b}{\bar{R}} + \frac{\bar{P}_v R_a}{\bar{R}} \quad (13)$$

The second factor in Eq. 13,  $P_v R_a / \bar{R}$ , is normally about 2 to 3 mm Hg while the first factor is about 70 mm Hg; thus neglecting the second factor in Eq. 13 in some case is permissible. The value of  $\bar{P}_g$  as determined from Eq. 13 can be checked by using Eq. 5 at points where  $\dot{P}_i$  is zero. Such points occur at peak systole and at end diastole and on occasions in mid systole and diastole. At such points the instantaneous flow is:

$$f = \frac{P_i - P_g}{R_a} \quad (14)$$

Solution for  $P_g$  at systole, end diastole, and for algebraic mean results in the following:

$$\begin{aligned} P_{gs} &= P_{is} - f_s R_a \quad \text{-- systolic} \\ P_{gd} &= P_{id} - f_d R_a \quad \text{-- diastolic} \\ P_{ga} &= \frac{P_{gs} + P_{gd}}{2} \quad \text{-- algebraic mean} \end{aligned} \quad (15)$$

where "s" and "d," respectively, refer to peak systole and end diastole. Because the resistance  $R_a$  decreases with increasing pressure it is probable that the estimate of  $P_{gs}$  is low and that of  $P_{gd}$  is high. The average of  $P_{gs}$  and  $P_{gd}$  can however serve as a check on the estimated mean glomerular capillary pressure.

From the model glomerular filtration rate (GFR) for one kidney can be defined as:

$$GFR = \frac{\bar{P}_g - \bar{P}_p}{R_g + R_p} \quad (16)$$

where  $\bar{P}_g$  and  $\bar{P}_p$  are respectively the glomerular filtration pressure and the tubular capillary pressure, and where  $R_g$  and  $R_p$  are resistance factors relating to glomerular and tubular capillary permeability. It may be valid to assume that the three factors  $R_g$ ,  $R_p$ , and  $\bar{P}_p$  are constant for many normal situations (Gomez, 1951). To determine the sum  $R_g$  and  $R_p$  it is necessary to obtain the GFR by renal plasma clearance techniques during which time the average glomerular filtration pressure is also determined. With the value of  $R_g + R_p$  established the instantaneous glomerular filtration rate can thereafter be directly determined from the instantaneous glomerular filtration pressure. The glomerular filtration pressure is available on a beat-to-beat basis and therefore the glomerular filtration rate is available on a beat-to-beat basis. Inspection of Eq. 7 also reveals techniques for determining the value of  $C_i$ . First at points where  $f$  is zero,  $R_a C_i$  can be determined from:

$$R_a C_i = - \dot{P}_i / \ddot{P}_i \quad (17)$$

Since  $R_a$  is known  $C_i$  can be calculated. Second, at points where  $\dot{P}_i$  is zero  $C_i$  is defined by:

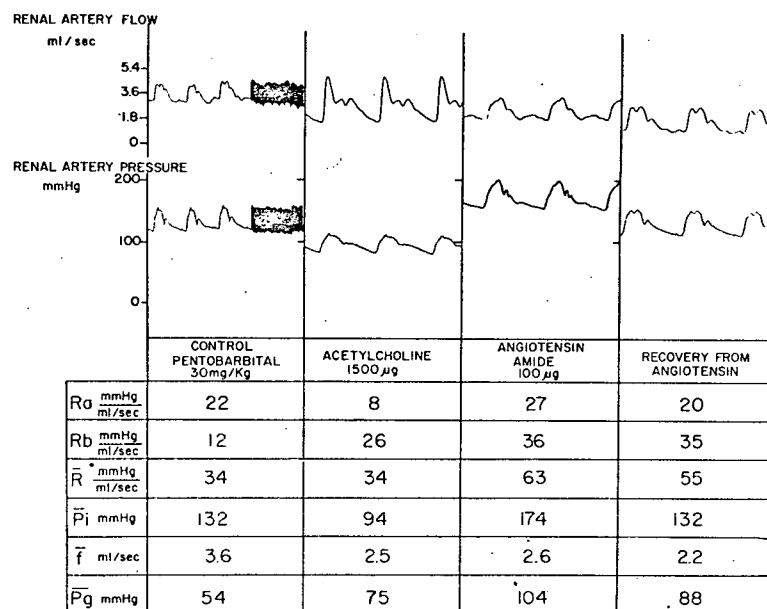
$$C_i = \dot{f} / \ddot{P}_i$$

(18)

This calculation point is marked by the right hand dashed line running through the curves in Fig. 10. Thus from measured values of pressure and flow,  $R_a$ ,  $C_i$ ,  $R_t + R_c$ , and  $\bar{P}_g$  can be derived.  $\bar{P}_g$  furnishes an estimate of instantaneous glomerular filtration rate. The compliance,  $C_i$ , yields information about the rigidity of the vascular walls. Since  $R_a$  is inversely proportional and compliance directly proportional to a power function of the conduit diameter, as resistance increases compliance decreases. This yields a valuable check on the directional changes in  $R_a$ . The elasticity of the vasculature, a major determinant of compliance, is influenced by the basic structure of the vessel walls and by the degree of smooth muscle activation. Arteriosclerosis modifies both the basic structure of the vessel walls and the amount of smooth muscle present. Thus the development of arteriosclerosis and atherosclerosis cannot be distinguished from sustained smooth muscle activation. However in the absence of smooth muscle activation the natural compliance can be determined and used as a measure of sclerotic development. Hinshaw *et al.* (1960) have suggested indications that the afferent arteriolar resistance may be mainly mediated by neurogenic factors, whereas, the efferent resistance may be mainly mediated by hormonal factors. These observations further suggest that segmental resistance values might be used to differentiate neurogenic and hormonal factors.

### C. Experimental Application in Renal Functions

Three dogs, each under different experimental circumstances, were used to develop and evaluate the basic concepts. An initial evaluation of the renal model was conducted using a dog anesthetized with 30 mg sodium pentobarbital per kilogram body weight. This dog had been implanted with a 6 mm lumen diameter flow probe several weeks prior to the experiment. Flow data was obtained by exteriorizing the connector and mating it to external electronics. Zero flow was established during injection of high concentrations of antiotensin amide. Pressure was obtained near the junction of the renal artery and the abdominal aorta via a P.E. 190 catheter connected to a P23 Db pressure transducer. Wave shapes and parameter values obtained during injection of angiotensin



\*WITH  $P_v$  ASSUMED TO BE 10mmHg

\*USDA\*

Figure 11. Pharmacological evaluation of renal model. Resistance  $R_a$  was estimated by dividing peak value of  $\bar{P}_i$  by peak values of  $\bar{f}$ . Calculation of all other values is according to equations presented in the text.

amide and acetylcholine are shown in Fig. 11. The pressure and flow wave forms are shown above each sequence. In this case  $R_a$  was determined by dividing peak  $\dot{P}_i$  by peak  $\dot{f}$ . This yields a value of  $R_a$  somewhat lower than that resulting from strict use of Eq. 8.

Under anesthesia a mean arterial pressure of 132 was recorded. Injection of acetylcholine resulted in an afferent resistance decrease to about 36% and a postglomerular value increase of 216% of the control value. The total resistance ( $R$ ) remained unchanged. Angiotensin amide produced an increase in all resistance values. The calculated mean glomerular capillary pressure varied throughout the experiment from 54 mm Hg to 104 mm Hg. Glomerular filtration rate was calculated from Eq. 16 using an assumed value for  $R_g$  of 70 mm Hg/ml/sec (1.17 mm Hg/ml/min).

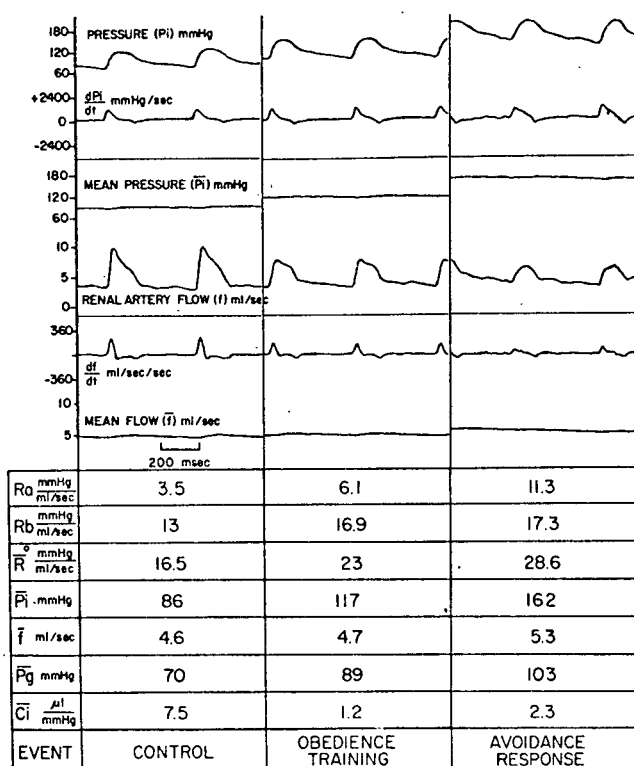
Figure 12a illustrates values obtained from a dog that was fully instrumented with an implantable pressure and flow telemetry system. This experimental sequence was designed to induce progressively increasing autonomic stimulation from control through avoidance behavior. In this case avoidance behavior was defined as the animal's reaction to the prospect of having the implant site touched. As the stimulation increased, the values calculated for all resistances increased. However the ratio of postglomerular to the total resistance did not change sufficiently to prevent an increase in the glomerular capillary pressure. With the assumption that  $R_g$ ,  $P_t$ , and  $\pi$  remained unchanged this stimulation caused an increase in the glomerular filtration rate. As compared to control value, the value calculated for  $C_i$  decreased for both the obedience training and the avoidance episode. The increase in  $C_i$  from obedience training to avoidance is probably associated with the increased pressure and thus an expansion of the vessel diameter preceding the afferent resistance site.

Figure 12b illustrates the recording obtained from this same dog at 0300, 0400, and 0500 hours during a period when records were taken each hour for a 24-hour period. The large amplitude, sharp flow characteristics tended to occur from 1100 to 0500 hours. The 0200-hour recording illustrates a period of low afferent resistance, the 0300-hour recording a period of low afferent resistance changing to a period of high afferent resistance, and the 0400-hour recording illustrates a period of sustained high afferent resistance. Although the value for compliance is not shown, inspection of the flow wave forms confirms that compliance is higher at 0300 hours than at 0500 hours.



Figure 12a. Progressive sympathetic arousal and its effect on renal parameters. From control through avoidance-reaction Ra increased to 320% and Rb to 135% of control values. In the same sequence, Pi increased to 189% and R to 170% of control values. Flow increased only slightly while Pg increased to 147% of control values. These parameter changes indicate that neuro-control resides primarily in the afferent resistance change; flow is well regulated, but the glomerular filtration pressure is variable.

Figure 12b. Spontaneous recordings. The left panel illustrates a period of low afferent resistance, the center recording illustrates a period of low afferent resistance changing to a higher value, the right panel illustrates a period during which the afferent resistance was sustained at a high level.



\* WITH  $P_v$  ASSUMED TO BE 10 mmHg  
 \* \* \* Rg \* \* \* 70 mmHg/ml/sec

\*MIKE\*

Figure 12a

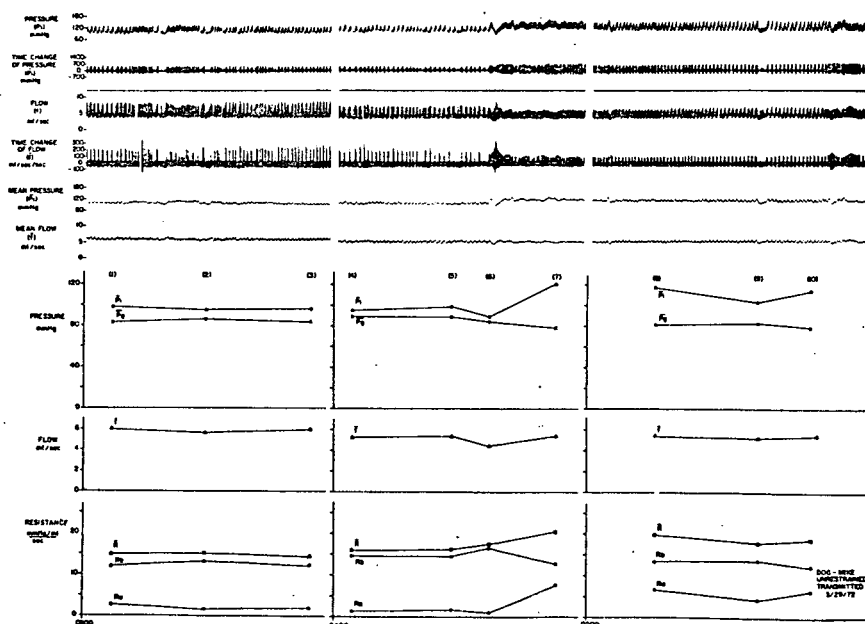


Figure 12b

Figure 13a illustrates data obtained from a third dog as he was recovering from halothane anesthesia following implantation of the electronics package. Under halothane a low afferent resistance value was calculated, whereas after partial recovery and when the subject was on ambient air, a large value of afferent resistance was calculated. Figure 13 shows tracing and resultant data obtained from this same dog at 2200 hours and at 1015 hours during a 24-hour data recording. The data taken at 2200 hours is indicative of a relatively dilated vascular system in contrast to the data recording at 1015 hours which indicates vasoconstriction.

#### D. Pitfalls and Problems

The best currently available implantable pressure transducers have drift characteristics which prevent long term use without periodic calibration. To reduce the magnitude of this problem it has been the practice to employ transducers certified by the manufacturer to have a baseline drift of less than 6 mm Hg per month and a sensitivity drift of less than  $\pm 3\%$  of the output at 200 mm Hg. In our experience in vivo sensor-drift characteristics have been somewhat greater than specified by the manufacturer. In this work calibration was conducted periodically by comparing transmitted pressures with pressures obtained by direct cannulation (Stevens, 1973, in press). A small polyethylene catheter connected to a pressure gauge is inserted via the femoral artery up to the level of the implanted transducer. Data is then recorded simultaneously from the implanted transmitter and the external pressure gauge. Systolic and diastolic pressure points on each record are assumed to be equal, hence a pressure voltage relationship for the transmitted data can be established. After the catheter removal the femoral vessel is repaired with fine sutures. This repair technique permits the calibration procedure to be conducted on one vessel many times.

Flow is calibrated before implant by forcing fluid through the flow probe lumen at several constant rates to develop a voltage output as a function of quantity of flow. An in vivo calibration is calculated by scaling the in vitro calibration by the ratio of lumen diameter to estimated vessel diameter. The zero baseline is estimated by injection of large quantities of hypertensin. This causes profound renal constriction and the minimum point on the flow during the lowest pressure is taken as the zero flow position.

Figure 13a. Cardiovascular response to Halothane. The left side shows recordings taken when the animal was on halothane and oxygen, the center is a transition period and the right side is a recording taken after the animal had been returned to ambient air.

Figure 13b. Comparison of renal parameter values determined when the animal was relaxed and alert.

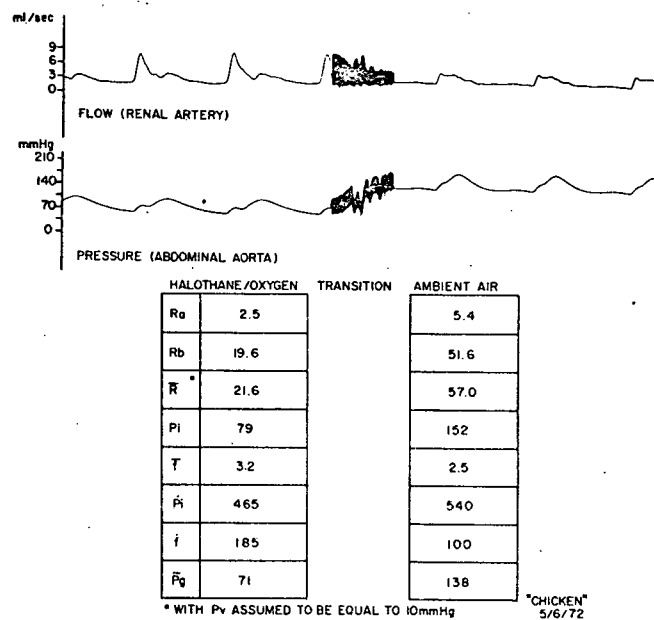


Figure 13a

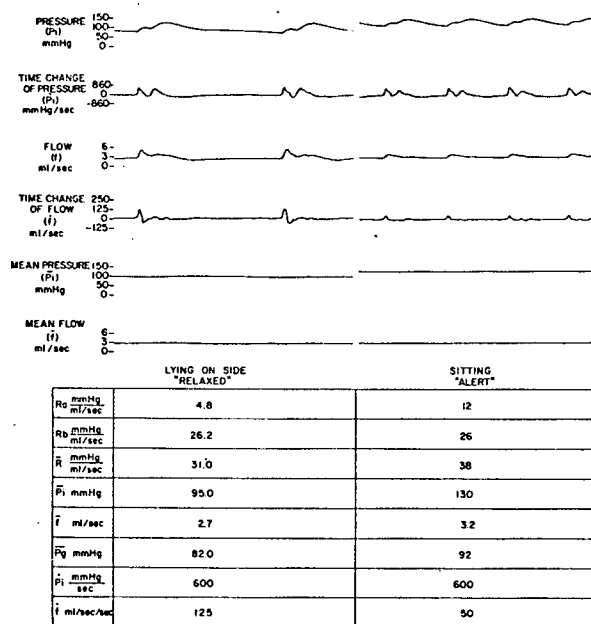


Figure 13b

Once the pressure sensitivity has been established by in vivo calibration, the error in  $R_a$  due to an error in  $\dot{P}_i$  can be assumed to be small, as the sensitivity will generally be less variable than the intercept. The major error in calculating both  $R_a$  and  $\bar{R}$  appears to be the flow sensitivity factor. Although no statistical evaluation has as yet been conducted, it is estimated that resistance values reported in this work are in error by  $\pm 25\%$ . These errors are mainly a product of applied techniques, not of limitations in the proposed approach. Pressure calibration has probably been realized to within  $\pm 5\%$  of the absolute value. However due to the unknown internal vessel diameter, flow sensitivity is probably in error by 20% of the absolute value. The adequacy of establishing zero flow by angiotensin injection has been confirmed by comparing zero flow levels in a sacrificed dog with flow levels produced by angiotensin in the same dog. These criteria yield an error in  $R_a$  and  $\bar{R}$  of  $\pm 25\%$ . The errors are in the same direction, thus the subtraction of  $R_a$  from  $\bar{R}$  to yield  $R_b$  is in error in the same direction by  $\pm 25\%$ . The error in the calculated values for  $R$ ,  $R_a$ , and  $R_t + R_c$ , does not produce equivalent errors in the calculated values for  $P_g$  and the GFR because resistance ratios are used in these calculations and the errors tend to cancel. It appears feasible to establish flow calibration within  $\pm 5\%$  of the absolute value by producing zero renal artery flow through the use of acetylcholine to stop the heart for a short period, or by eliciting profound renal constriction through the use of angiotensin, and by establishing flow sensitivity by comparing values of flow measure with the telemetry system with values measured by clearance techniques. On the basis of the model, resistance values can then be determined to within  $\pm 10\%$ . With this degree of potential accuracy present in electronic techniques the adequacy of the model must be further evaluated. In discussing the previous model it has been assumed that the components' values do not vary with pressure, that the components' values can be lumped, and that the mass of blood is negligible. If the parameter variation with pressure is ignored but the mass of the blood is included, the renal flow is given by:

$$\dot{f} = C_i \dot{P}_i - M C_i \ddot{f} + \frac{P_i - P_g - M \dot{f}}{R_a} \quad (19)$$

where  $M$  is a factor related to the mass of the blood. In the model this would appear as an inductor preceding the compliance  $C_i$ . Differentiation of Eq. 19 yields:

$$\dot{f} = C_i \ddot{P}_i - M C_i \ddot{f} + \frac{\dot{P}_i}{R_a} - \frac{\dot{P}_g}{R_a} - \frac{M \ddot{f}}{R_a} \quad (20)$$

At points where  $\dot{P}_i$  is zero, i.e., maximum and minimum points of  $\dot{P}_i$ , the first term on the right of the equal signs vanishes. As before, it is assumed that the term  $\dot{P}_g/R_a$  can be neglected because of the large compliance in the glomeruli. The approximate equation for  $R_a$  when inertia of the blood is included is thus:

$$R_a = \frac{\dot{P}_i - M \ddot{f}}{\dot{f} + M C_i \ddot{f}} \quad \text{at maximum and minimums of } \dot{P}_i \quad (21)$$

If  $M$  has an appreciable value, the determination of  $R_a$  by Eq. 21 will be substantially larger than the determination by Eq. 8. To determine  $R_a$  from Eq. 21 a value of  $M$  must be assumed. Rothe and Williams (1972) report a value of 0.05 mm Hg - sec<sup>2</sup>/ml for  $M$  and a value of 0.001 ml/mm Hg for the compliance  $C_i$ . Our measurements indicate that at the point where  $\dot{P}_i$  is a maximum, i.e., at the inflection point of  $\dot{P}_i$ , the values of  $\dot{f}$ ,  $\ddot{f}$  and  $\ddot{f}$  are 100 ml/sec<sup>2</sup>, -7000 ml/sec<sup>3</sup>, and -700,000 ml/sec<sup>4</sup>, respectively. The products  $M \ddot{f}$  and  $M C_i \ddot{f}$  are -350 mm Hg/sec<sup>2</sup> and -35 ml/sec<sup>2</sup>, respectively. The value of  $\dot{P}_i$  at this point is on the order of 800 mm Hg/sec. Using these values, application of Eqs. 8 and 21 yields values for  $R_a$  of 8 and 17.5, respectively. Thus, on the basis of the approximate value listed above Eq. 8 will yield a value for  $R_a$  on the order of 50% lower than Eq. 21. Since errors in the calculated value of  $R_a$  inject errors into the determinations of postglomerular resistance  $R_b$ , glomerular filtration pressure  $\dot{P}_g$ , and the filtration resistance  $R_g$ , it is important to appreciate the possible effects of ignoring the mass of the blood in renal hemodynamic investigations. From Eq. 20 at points where  $\dot{P}_i = 0$  with the assumption that  $M \ddot{f}$  and  $M C_i \ddot{f}$  are negligible the compliance is defined by:

$$C_i = \dot{f} / \ddot{P}_i \quad (\dot{P}_i = 0) \quad (22)$$

The estimation of  $C_i$  from Equation 22 appears to be reasonable as neither  $\dot{P}$  nor  $\dot{f}$  are changing rapidly and a moderate phase shift between  $\dot{f}$  and  $\dot{P}_i$  would not cause appreciable error. The assumption that factors containing  $\ddot{f}$  and  $\ddot{f}$  can be neglected in calculation the compliance is valid, as in the vicinity of  $\dot{P}_i = 0$   $\dot{f}$  is nearly constant, and thus  $\ddot{f}$  and  $\ddot{f}$  are nearly zero.

The value for  $C_i$  estimated during pentobarbital anesthesia is considerably lower than the value estimated during unrestrained natural activity. The value determined when subjects are anesthetized with pentobarbital approximates that estimated by Rothe under similar conditions. However, even though the estimate of compliance by Eq. 22 appears to be accurate, care must be exercised in applying Eq. 21 to determine  $R_a$ . The curve shown in Fig. 10 illustrates that at the inflection point of  $\bar{f}$  the value of  $\bar{f}$  is approximately 100. But  $\dot{P}_i$  is approaching a maximum rapidly, and thus  $P_i$  is approaching a zero value rapidly. Thus any phase shifts between pressure and flow due to sensor placement, the hydraulics of the pressure-sensing system, or the electronics will cause a serious error in the calculation of  $R_a$  because of the influence this has on the value of  $\dot{P}_i$ . An estimate of the minimum acceptable phase error is available from the fact that flow rises from a diastolic level to a peak systolic level often in less than 40 msec. Thus for reasonable results using the suggested calculations, the time shift between the two parameters caused by artifacts must be maintained quite small. The value for  $\bar{f}$  determined by integrating Eq. 19 is:

$$\bar{f} = \frac{1}{T_2 - T_1} \int_{T_2}^{T_1} \left[ C_i \dot{P}_i - M C_i \ddot{f} + \frac{1}{R_a} (P_i - P_g - M \ddot{f}) \right] dt \quad (23)$$

The integrals of the first, second, and last terms are zero. The mean difference pressure and the resistance contribute to the mean flow value and the mean resistance  $\bar{R}$  is the same as that in the model which neglected the mass of this blood. Thus  $\bar{R}$  is influenced mainly by errors in pressure and flow measurement and not by model inconsistencies.

#### E. Discussion

The character of the flow when the effects of pentobarbital are likely the most influential, i.e. far left and far right, in Fig. 11 is consistent with the sympathomimetic effect of pentobarbital. The altered character of the flow in the case where the effects of angiotensin amide are added to the pentobarbital is produced by even greater vasoconstriction. The wave flow shape in this case is quite similar to the wave shape of the pressure, indicating a very rigid renal vascular system. Flow wave shapes occurring in constricted vessels can be contrasted with the wave shapes generated when



acetylcholine is the dominant pharmacologic agent. In this case pressure and flow are both down from precontrol values. The afferent resistance is down and the postglomerular resistance is up. Dilatation of the afferent resistance is likely due to the direct effect of acetylcholine on the smooth muscle and to the cholinergic neurodilatation effect on the kidney (Stinson *et al.*, 1969). The mechanism causing the increase in the postglomerular resistance is not understood, but the result is maintenance of glomerular pressure in the face of declining systemic pressure.

Figure 13a can be compared to Fig. 11 to contrast the effects of halothane and the barbiturates. The hypotensive effects of halothane are evident; pressure and the afferent resistance are both low and the characteristic of the flow is that of pulsatile flow through distensible vessels. It can be concluded that the renal vascular system is quite compliant under the effects of halothane. The gradual shift from the distensible appearance to the rigid appearance during the transformation from halothane and oxygen to ambient air is quite noticeable. The increase in total and postglomerular resistance is particularly large during this transition.

The three sections in Fig. 12a illustrate three degrees of "sympathetic arousal." This degree of arousal is subjective as no measurement of neuroactivity was performed. An important observation to be made in this figure is that the afferent resistance values increase by a factor of 3, whereas, the postglomerular resistance increases by only 1.3. It is likely that these changes are mediated by neurogenic activity as the change from the dilated renal vasculature, as it appears in the control section, to the constricted appearance, as exemplified by the avoidance reaction, occurred in a matter of 8 to 12 heartbeats. This appears to be insufficient time for adrenal medullary hormones to have played a significant role in the responses. Figure 12b illustrates a spontaneous change in parameters recorded on many occasions during 24-hour baseline data acquisition tests. These episodes are characterized by a very compliant renal vasculature changing to a considerably less compliant appearance without a noticeable change in subject behavior. It is suggested that these very relaxed episodes may be in synchrony with rapid eye movement (REM) sleep.

The respiratory influence on the renal hemodynamics can also be seen in the data illustrated in Fig. 12b. As the pressure decreases with the respiratory cycle the value of  $R_a$

also decreases. Brief episodes of a sustained decrease in Ra when the pressure is sustained at a low level are also evident at several points throughout these recordings. Note particularly points 2, 6, 9, and 10. During these sustained low pressure events Ra tends to show a linear decrease in value with time.

A shoulder on the systolic portion of the pressure wave is seen in many dogs. For the dog called Mike this shoulder developed after about one month of implant. After appearing it was most evident during relaxed episodes. For the dog called Chicken the shoulder often developed into a valley during vasodilatation (Fig. 13a left). A question arises as to whether this is a natural phenomenon or whether it is associated with instrumentation artifacts. The placement of the transducer to detect lateral pressure rather than end pressure creates the possibility of an artifact associated with the cooling effect of the high velocity blood flow on the sensing elements of the transducer. Based on the placement of the pressure sensor at 20 mm downstream from the renal artery and a pressure pulse velocity of 4 msec, the artifact due to a cooling effect would occur approximately 5 msec after the peak flow into the renal artery. However this shoulder always appears to occur several tens of msec after peak flow velocity is attained by the kidney. This observation does not support the contention that the shoulder is produced by the instrumentation artifact.

O'Rourke and Taylor (1966) have also observed this shoulder and conclude that it is a consequence of the properties of the vascular system. Rothe and Nash (1968) have concluded that the notch is real as it produces renal flow of the proper phase and magnitude. Our data would further suggest that the shoulder is a consequence of the properties of the vascular system as it does not appear to bear the proper phase relationship to an artifact generated by a potential cooling effect and furthermore its magnitude and position appear to be closely associated with the tone of the vascular system. As the vascular tone increases, the period of an oscillation produced by the systolic shock wave could be expected to decrease. This trend is apparent in Figs. 13a and 13b where the shift in position due to changing tone is as much as 40 msec. It appears most likely that this shoulder is produced by reflections from bifurcations as the change in its position with a change in tone and, thus, a change in the pressure pulse velocity could be on the order of 100 msec.

On the basis of the model and the data analysis four factors emerge: (1) postglomerular resistances are strongly influenced by blood-borne hormonal factors but appear not to be under strong neurogenic control, (2) afferent resistances are under considerable autonomic control and in addition they are sharply mediated by the exogenous circulating hormones which were tested, (3) flow is less well regulated under hormonal manipulation than neurogenic manipulation, and (4) glomerular filtration rate is influenced by both sympathetic arousal and the more chronic hormonal factors. It also appears that the afferent resistance occurring during very relaxed periods approaches the value produced by exogenous acetylcholine and by halothane anesthesia.

Folkow and Neil (1971) have reported that hypertensive rats exhibit vascular resistances higher than normotensive rats even at maximum vasodilatation. Thus in any particular animal sclerotic developments could be verified by measuring the afferent resistance when the autoregulatory phenomenon of the kidney has been neutralized by smooth muscle relaxants. The position of the shoulder previously mentioned might be used as an index of the tone of the large vessels in the systemic circulation. Thus sclerotic development in the large vessels might be tracked distinctly from the same development in the renal system. It also appears that a relative index of stroke volume is available from consideration of both the maximum  $dp/dt$  and the position of the shoulder relative to systolic onset. With the assumption that the period of oscillation in a damped oscillatory system is independent of magnitude of shock, then the position of the shoulder is affected only by the elasticity of the vascular system. The time rate of pressure change is a function of both the elasticity of the vascular system and the stroke volume of the heart. This can be formulated as follows:

$$\dot{P}_i = f(\Delta T, S.V.) \quad (24)$$

where S.V. is stroke volume,  $\Delta T$  is time from onset of systole to appearance of shoulder and  $\dot{P}_i$  is the time rate of pressure change and  $f$  denotes "a function of." Therefore if the position of the shoulder remains unchanged,  $\Delta T$  is constant, but  $\dot{P}_i$  increases, it may mean that the elasticity has not changed, but the stroke volume has increased. If the position of the shoulder changes, then with constant stroke volume output  $\dot{P}_i$  may have changed. If it doesn't, stroke volume has necessarily changed. Thus for researching the genesis of hypertension this impedance technique appears to have particular relevance.

- F. References (Section III - Cardiovascular Research Applications)
- Folkow, Björn and Neil, Eric (1971). Circulation. Oxford University Press, New York.
- Gómez, Domingo M. (1951). "Evaluation of Renal Resistances, with Special Reference to Changes in Essential Hypertension." J Clin Invest 30:1143-1155.
- Henry, James P. and Meehan, John P. (1971). The Circulation: An Integrative Physiologic Study. Year Book Medical Publishers, Chicago.
- Hinshaw, Lerner B., Flaig, Robert D., Carlson, Curtis H., and Thuong, Nguyen K. (1960). "Pre- and Postglomerular Resistance Changes in the Isolated Perfused Kidney." Am J Physiol 199(5):923-926.
- O'Rourke, M. F. and Taylor, M. G. (1966). "Vascular Impedance of the Femoral Bed." Cir Res 18:126-139.
- Rader, R. D., Stevens, C. M., Henry, J. P., and Meehan, John P. "Use of Implanted Telemetry in Vascular Research." Proc 1972 International Telemetering Conf (Oct 10-12, Los Angeles) 8:487-498.
- Rothe, Carl F. and Nash, Franklin D. (1968). "Renal Arterial Compliance and Conductance Measurement Using on-Line Self-Adaptive Analog Computation of Model Parameters." Med Biol Eng 6:53-69.
- Rothe, Carl F. and Williams, Bruce P. (1972). "Dynamic Characteristics of the Renal Arterial Microvasculature of the Dog Obtained by Simulation." IEEE Trans Biomed Eng BME-19(3):213-221 (May).
- Stevens, Christopher M., Meehan, John P., and Rader, Roland D. (In press, 1973). "Blood Pressure Measurement with Chronically Implanted, Intravascular Transducers," In Ernest P. McCutcheon (ed.), Implanted Cardiovascular Instrumentation, Academic Press, New York, chap 26.
- Stinson, J. M., Barnes, A. B., Zakheim, R. M., Chimoskey, J. E., Spinelli, F. R., and Barger, A. C. (1969). "Reflex Cholinergic Vasodilatation during Renal Artery Constriction in the Unanesthetized Dog." Am J Physiol 217:239-246.
- Thompson, David Elton (1970). The Fluid Dynamics of Renal Blood Flow. Ph.D. dissertation, Purdue University, Lafayette, Ind., January.

#### IV. Conclusions

The advantages of a telemetry system for measurement of cardiovascular parameters has been considered in some detail. It is clear that many experiments can be conducted effectively only when aided by telemetry techniques. Certainly telemetry has a unique potential for cutting through the complex problem of separating psychological factors from the physiological parameters under investigation. In fact, it greatly simplifies the problem of carrying out physiological experiments on conscious subjects while still controlling emotional variables. The advantages of using remote recording in studies which demand complete relaxation and freedom of the animal to interact socially are evident. Telemetry also expands the latitude for investigating the cardiovascular responses under broad environmental conditions; and it appears that if the effects of long term weightlessness on cardiovascular dynamics are to be thoroughly investigated, telemetry offers an improved approach.

The implanted miniaturized system described in this report goes one step further in eliminating the clouding of the data by unwanted emotional responses which are more likely to occur in animals with external telemetry and hardwire procedures. Thus it permits a more valid interpretation of the influence of the manipulated variable on physiological functions. The implant method also allows a better definition of normal physiological baseline conditions and eliminates many troublesome problems associated with both hardwire and external telemetry techniques. Thus the equipment described appears to have widespread applicability in chronic studies dealing with cardiovascular adjustments to various stresses.

Although the implant technique has progressed rapidly during the past 10 years, the process of refinement is not completed. Long term stability must be improved. For flow in the system described there is a sensitivity imprecision (volts/ml/sec) of near  $\pm 10\%$  which is related to the inability to either measure or know absolute values of the system's parameters, mainly the sound velocity and vessel internal diameter, to a sufficient degree of precision. Calibration of the entire system as a function of milliliters of blood per second forced through a vessel similar to the vessel on which eventual measurement will be conducted can theoretically eliminate this imprecision. However the vessel diameter can not necessarily be assumed to be the same in an in vivo application; thus the calibration is not reliably translatable to

the final flow measurement. Real sensitivity is a direct function of the vessel diameter which varies in experimental situations. The stability of the sensitivity, assuming a fixed diameter, is quite good. It is mainly a function of the system balance and the differential change in crystal impedance. By application of the limiting concept amplitude instabilities can be substantially reduced. Change in velocity of ultrasound with temperature is minimal. The final conclusion regarding sensitivity stability is that it is a major function of the internal vessel diameter and is reasonably independent of other factors.

The position of the intercept (zero flow output voltage) with voltage limits incorporated is mainly influenced by varying crystal properties which induce differential phase changes. It is not known what these differential phase changes are in relation to long term aging of the crystals, for this factor has not yet been investigated. The relative phase change caused by temperature and media change is related to differential variation in resistive and reactive components of the crystals and has been experimentally determined to be short 1% of fullscale per degree Centigrade. The output voltage for zero flow is established when there is zero flow of normal blood at a constant temperature.

For normal implant operation where the environmental temperature is expected to vary little the maximum possible change would be from 94 to 104 degrees Fahrenheit; for such a rare event, the baseline would vary by no more than 10% of fullscale. More typical operations would yield a 3% to 6% precision for baseline conditions. This stability is obtained with very low power consumption and modest circuitry. The final conclusion is that for chronic implants, where long term stability in conjunction with low power consumption and small size is a requirement, the interferometric ultrasonic flow technique is an improvement over other available techniques.

Presently there appears to be no satisfactory alternate to the miniature implanted solid state transducer for measuring blood pressure. As previously mentioned in Section 1 a total error of 12 mm Hg per month would not be unusual. This error can be narrowed considerably in establishing calibration by comparing transmitted pressure to pressure obtained by cannulation.

Implant telemetry is currently being employed in projects to determine the physiological responses to prolonged stress, in establishing the normal for physiological values in animals which are traditionally used in research, and in the military sentry dog program to optimize obedience training programs. Within the next 10 years, sensors allowing chronic measurement of chemical constituents will be added to the repertory. Despite high initial expense of an implantable telemetry system, it may in the long run prove to be quite efficient as the experimenter will be able to conduct multiple experiments on one animal without compromise to the others. As an example, chronic emotional stress and physical stress studies could be conducted in parallel.

Since it is feasible to study renal hemodynamics by the application of impedance determining techniques to measured values of pressure and flow, one can now calculate the total resistance to flow as well as the pre- and postglomerular resistance values and the final outcome is an estimate of filtration rate and an indication of neurogenic and hormonal drive levels.

Present data suggest that neurogenic and humorally mediated vascular adjustments will occur in response to long term weightlessness. The renal regulation of sodium, potassium, and water in response to a shift of blood volume to the thorax is a proposed central factor in these adjustments. Expansion of the atria due to the shift of blood to the thorax results in a reduction in sympathetic outflow to the smooth muscle of the kidney, producing a decrease in pre-glomerular resistance and an increase in glomerular filtration rate. This sympathetic outflow is also responsive to a variety of psychological and environmental stimuli (pain, fright, exercise, restraint, etc.) which may alter fluid and electrolyte balance through modification of renal vascular resistance. The ability to determine specific values of renal impedance permits the filtration pressure and the filtration rate to be estimated and because of the differential humoral neurocontrol it may also be feasible to determine the specific cause of the component changes without chemical assays. In long term orbital experiments the ability to perform renal function studies without chemical assays has considerable impact on weight, power, size, and reliability factors.

## A c k n o w l e d g m e n t s

The assistance of co-workers John Henriksen, Leo Casados, and John Henry in circuit development and packaging and the aid in instrument application and evaluation by Dr. C. M. Stevens, also of the U.S.C. Department of Physiology, and by Majors William Sears, Robert Krutz, and Richard Trumbo of the U.S. Air Force is gratefully acknowledged. Sincere appreciation is also extended to Jo Kolsum for typing the manuscript and for her assistance in the final editing.